Published for SISSA by Springer

Received: October 26, 2023
Accepted: January 20, 2024
Published: February 9, 2024

Prompt and non-prompt J/ψ production at midrapidity in Pb–Pb collisions at $\sqrt{s_{\rm NN}} = 5.02$ TeV

The ALICE collaboration

E-mail: ALICE-publications@cern.ch

Abstract: The transverse momentum ($p_{\rm T}$) and centrality dependence of the nuclear modification factor $R_{\rm AA}$ of prompt and non-prompt J/ψ, the latter originating from the weak decays of beauty hadrons, have been measured by the ALICE collaboration in Pb–Pb collisions at $\sqrt{s_{\rm NN}} = 5.02$ TeV. The measurements are carried out through the $\rm e^+e^-$ decay channel at midrapidity ($|y| < 0.9$) in the transverse momentum region $1.5 < p_{\rm T} < 10$ GeV/c. Both prompt and non-prompt J/ψ measurements indicate a significant suppression for $p_{\rm T} > 5$ GeV/c, which becomes stronger with increasing collision centrality. The results are consistent with similar LHC measurements in the overlapping $p_{\rm T}$ intervals, and cover the kinematic region down to $p_{\rm T} = 1.5$ GeV/c at midrapidity, not accessible by other LHC experiments. The suppression of prompt J/ψ in central and semicentral collisions exhibits a decreasing trend towards lower transverse momentum, described within uncertainties by models implementing J/ψ production from recombination of c and $\bar{\rm c}$ quarks produced independently in different partonic scatterings. At high transverse momentum, transport models including quarkonium dissociation are able to describe the suppression for prompt J/ψ. For non-prompt J/ψ, the suppression predicted by models including both collisional and radiative processes for the computation of the beauty-quark energy loss inside the quark-gluon plasma is consistent with measurements within uncertainties.

Keywords: Heavy Ion Experiments, Heavy Quark Production, Quarkonium

ArXiv ePrint: 2308.16125

https://doi.org/10.1007/JHEP02(2024)066

JHEP02(2024)066

Contents

1 Introduction

Quantum chromodynamics (QCD) calculations on the lattice [1–4] predict the existence of the quark-gluon plasma (QGP), a state of strongly-interacting matter characterised by quark and gluon degrees of freedom, expected to be produced at extremely high temperatures and energy densities. Such conditions can be realised in the laboratory by colliding heavy ions at ultra-relativistic energies, enabling the study of the properties of this state of matter, as shown by multiple measurements carried out at the SPS [5, 6], RHIC [7–10] and LHC [11]. Heavy quarks, i.e. charm and beauty, are mainly produced in hard parton-parton scatterings and on a shorter time scale than the QGP formation time at LHC energies ($\tau_{\text{QGP}} \approx 1.5\,\text{fm}/c$) [12, 13], thus experiencing the full QGP evolution. Charmonia, bound states of a charm and an anti-charm quark, are interesting probes of the QGP. In fact, it was predicted that their production would be suppressed in this medium due to static colour screening resulting from the high density of colour charges inside it [14] or due to dynamical dissociation [15]. A suppression of the J/ψ yield in heavy-ion collisions relative to proton-proton collisions was observed at the SPS [16, 17], RHIC [18–21] and LHC [22–31]. However, at LHC energies, the J/ψ suppression is significantly reduced compared to lower energy results, in particular at low transverse momentum (p_{T}) and in more central collisions. These findings are interpreted by considering an additional contribution to the J/ψ production, known as regeneration, according to which the abundantly produced charm and anti-charm quarks from different hard partonic scatterings can recombine to form charmonium states [32, 33]. Previous ALICE inclusive J/ψ measurements at both central and forward rapidity, which have revealed significantly less

JHEP02(2024)066

suppression of J/ψ at low transverse momentum compared to lower energies [27, 28, 31] as well as non-zero elliptic flow [34, 35], have clearly demonstrated the relevance of this mechanism.

Different phenomenological scenarios are assumed for the description of charmonium production in heavy-ion collisions. In the Statistical Hadronisation model [32, 36], the abundances of all charmonium states are determined by thermal weights at the chemical freeze-out. By contrast, according to several partonic transport models [33, 37, 38] the charmonium states can be produced via regeneration throughout the full evolution of the QGP phase. Recent inclusive J/ψ results in Pb–Pb collisions at $\sqrt{s_{\rm NN}} = 5.02$ TeV indicate that both approaches can provide a description of the measured suppression within uncertainties in the low-$p_{\rm T}$ region [27, 28, 31]. Results of $\psi(2S)$ suppression recently released by the ALICE collaboration [39] show that transport models better reproduce charmonium measurements for central events compared to the Statistical Hadronisation model. Besides providing a good description of the production, transport models are also able to describe the elliptic flow of inclusive J/ψ [34, 40]. As the $p_{\rm T}$ of the J/ψ increases, the contribution from regeneration becomes less relevant, while charmonium dissociation and fragmentation of high-energy partons into charmonia become dominant.

Inclusive J/ψ production in high-energy hadronic collisions consists of several contributions: the J/ψ produced directly and from the decays of higher mass charmonium states (e.g. ψ(2S) or $\chi_{\rm c}$), known as the "prompt" contribution, and J/ψ originating from the weak decays of beauty hadrons. The latter component, referred to as "non-prompt", is characterised by a production vertex displaced with respect to the primary vertex of the collision, and this feature is exploited experimentally to separate the two contributions. The measurement of prompt J/ψ production enables a direct comparison with prompt charmonium models. In addition, the non-prompt J/ψ production measurement grants a direct insight into the suppression of beauty hadrons, which are expected to be sensitive to the properties of the medium created in heavy-ion collisions as ancestor beauty quarks experience energy loss by interacting with QGP constituents. The energy loss of partons inside the medium is expected to happen via both radiative [41, 42] and elastic collisional processes [43–45]. The relative contribution of the former is expected to increase with $p_{\rm T}$. The energy loss strongly depends on the colour charge of the parton, being larger for gluons than for quarks, as well as on the parton mass [46–48]. The production of open heavy-flavour hadrons in nuclear collisions is also affected by in-medium hadronisation effects. Due to the high quark density in the QGP, heavy quarks can also hadronise via coalescence, by recombining with other light flavour quarks inside the medium [49–51].

In order to interpret both prompt and non-prompt J/ψ results in nuclear collisions, cold nuclear matter (CNM) effects need to be considered. The main effect at LHC energies is represented by the modification of the parton distribution functions of protons and neutrons inside nuclei compared to the ones of the free nucleons [52]. These effects are usually addressed through measurements in proton-nucleus collisions at the same centre-of-mass energy and are expected to be effective below 3 GeV/c for prompt J/ψ, as shown by recent J/ψ results in p–Pb collisions at $\sqrt{s_{\rm NN}} = 5.02$ TeV [53]. For non-prompt J/ψ, a small suppression with no significant $p_{\rm T}$ dependence is observed, although with large uncertainties [53].

JHEP02(2024)066

At LHC energies in heavy-ion collisions, the production of prompt and non-prompt J/ψ was measured at midrapidity by the CMS [22] and ALICE [54] collaborations in Pb–Pb collisions at $\sqrt{s_{\rm NN}} = 2.76$ TeV. At the centre-of-mass energy of $\sqrt{s_{\rm NN}} = 5.02$ TeV in the central rapidity region, the ATLAS [29] and CMS [30] collaborations measured the suppression of prompt and non-prompt J/ψ at high transverse momentum. At low $p_{\rm T}$, inclusive J/ψ measurements were carried out by the ALICE collaboration [28, 31]. In this article, $p_{\rm T}$ and centrality dependent measurements of prompt and non-prompt J/ψ production at midrapidity in Pb–Pb collisions at $\sqrt{s_{\rm NN}} = 5.02$ TeV are presented. These results, obtained down to $p_{\rm T} = 1.5\,{\rm GeV}/c$, have a unique kinematic coverage at the LHC compared to existing midrapidity measurements at the same centre-of-mass energy, which are available only at high transverse momentum. Furthermore, they have a significantly improved precision compared to previous published ALICE results at lower energy.

This article is organised as follows: the ALICE apparatus and data samples are described in section 2, the analysis technique is presented in section 3, results and comparison with similar measurements from other experiments and model calculations are discussed in section 4, and finally the summary is provided in section 5.

2 Experimental apparatus and data sample

The ALICE detector consists of a central barrel with a pseudorapidity coverage of $|\eta| < 0.9$ and a forward rapidity muon spectrometer with a pseudorapidity coverage for muons of $-4 < \eta < -2.5$. It also includes forward and backward pseudorapidity detectors employed for triggering, background rejection, and event characterisation. Central barrel detectors are placed inside a magnetic field $B = 0.5$ T provided by a solenoidal magnet. A complete description of the detector and an overview of its performance are discussed in refs. [55, 56]. The main detectors employed for the analysis described in this article are the Inner Tracking System (ITS) [56], the Time Projection Chamber (TPC) [57] and the V0 detector [58]. Both ITS and TPC detectors enable the measurement of inclusive J/ψ mesons via the dielectron decay channel in the central rapidity region down to zero $p_{\rm T}$. The ITS consists of six layers of silicon detectors, with the two innermost layers composed of silicon pixel detectors (SPD) which provide the spatial resolution to separate prompt and non-prompt J/ψ on a statistical basis. The TPC is the main tracking detector of the central barrel. In addition, it allows for particle identification via the measurement of the specific ionisation energy loss ${\rm d}E/{\rm d}x$ in the detector gas. The V0 detector consists of two scintillator arrays placed on each side of the interaction point (with pseudorapidity coverage $2.8 < \eta < 5.1$ and $-3.7 < \eta < -1.7$), and it is used to reject offline beam-induced background events, to define a minimum bias trigger, and to characterise the event centrality. The zero degree calorimeters [59], located at ± 112.5 m on both sides of the interaction point, are used to reject electromagnetic interactions and beam-induced background in Pb–Pb collisions. The results presented in this article are based on the same data samples of Pb–Pb collisions at $\sqrt{s_{\rm NN}} = 5.02$ TeV employed for the inclusive J/ψ analysis [31]. In particular, it consist of a combination of the data samples collected during the years 2015 and 2018 of the LHC Run 2. In order to obtain a uniform acceptance of the detectors, only events with a reconstructed primary vertex position along the beam line located within ± 10 cm from the centre of the detector were considered. In addition,

JHEP02(2024)066

consecutive events triggered within a time interval smaller than the readout time of the TPC were discarded as these are expected to have a high total charge deposition in the active volume and consequently significantly worse particle identification performance of the TPC. The datasets are collected with a minimum bias triggered event sample, provided by the coincidence of signals in the two scintillator arrays of the V0 detector. The corresponding integrated luminosity is about 24 μb^{-1} [60]. In addition, centrality triggered samples, whose trigger definition is based on the amplitude of the signal collected in the V0 detector, were used. These correspond to central (0–10%) and semicentral (30–50%) events, equivalent to an integrated luminosity of 105 and 51 μb^{-1} [60], respectively.

3 Data analysis

In order to estimate hot nuclear matter effects, the nuclear modification factor can be defined as the production yield in Pb–Pb collisions at $\sqrt{s_{NN}} = 5.02$ TeV normalised to the reference production cross section in pp collisions at the same energy and scaled by the average nuclear overlap function $\langle T_{AA} \rangle$ [60]:

$$R_{AA} = \frac{dN/dp_T dy}{\langle T_{AA} \rangle \times d\sigma_{pp}/dp_T dy}. \tag{3.1}$$

Inclusive J/ψ measurements with no separation between prompt and non-prompt contributions are carried out by the ALICE collaboration at midrapidity ($|y| < 0.9$) in Pb–Pb collisions at $\sqrt{s_{NN}} = 5.02$ TeV, as discussed in ref. [31]. The nuclear modification factors of prompt and non-prompt J/ψ at midrapidity can be obtained by combining inclusive J/ψ R_{AA} measurements with non-prompt J/ψ fractions (f_B), the latter defined as the ratios of the production yields of J/ψ mesons originating from beauty-hadron decays to that of inclusive J/ψ, estimated in both Pb–Pb collisions and pp collisions at the same centre-of-mass energy.

3.1 Non-prompt J/ψ analysis in Pb–Pb collisions

Selection of J/ψ candidates. The event selection and track quality requirements used in the analysis discussed in this article are identical to those used for the corresponding midrapidity inclusive J/ψ R_{AA} analysis in Pb–Pb collisions at $\sqrt{s_{NN}} = 5.02$ TeV [31]. Prompt and non-prompt J/ψ measurements are carried out in the J/ψ transverse momentum interval 1.5–10 GeV/c and in four different centrality classes, namely 0–10%, 10–30%, 30–50%, and 50–90%. The results are presented as a function of the transverse momentum of the J/ψ, as well as of the average number of participants ($\langle N_{part} \rangle$). The latter can be estimated via Glauber model calculations [61–64] for the different centrality intervals [60].

J/ψ candidates are reconstructed at midrapidity ($|y| < 0.9$) through the dielectron decay channel. Electron candidates, reconstructed using both ITS and TPC detectors, are required to have a pseudorapidity in the interval $|\eta| < 0.9$, a minimum transverse momentum of 1 GeV/c, and a minimum of 70 space points out of a maximum of 159 in the TPC. A hit in at least one of the two SPD layers is also required to improve the tracking and the spatial resolution. Several quality selection criteria, also employed for the inclusive J/ψ analysis [31], are considered in order to ensure good track resolution, as well as to reduce the contribution of electrons and positrons originating from photon conversion in the detector material and to

JHEP02(2024)066

reject secondary tracks originating from weak decays. The electron identification relies on the measurement of $\mathrm{d}E/\mathrm{d}x$ in the TPC, using stricter requirements than those considered for the inclusive J/ψ analysis in order to increase the signal-to-background ratio, in particular at low transverse momentum and in central events. For tracks reconstructed in more peripheral centrality classes, namely 30–50% and 50–90%, the TPC $\mathrm{d}E/\mathrm{d}x$ signal is required to lie within the interval $[-3, 3]\sigma_{\mathrm{e}}$ relative to the expectation for electrons, where σ_{e} represents the specific energy-loss resolution for electrons in the TPC. In addition, tracks consistent with the pion and proton assumptions within 3.5σ are rejected. For the centrality classes 0–10% and 10–30%, the electron inclusion is requested to be $[-2, 3]\sigma_{\mathrm{e}}$ ($[-1, 3]\sigma_{\mathrm{e}}$) for the p_{T} of the electron below (above) 5 GeV/c. A 4.5σ rejection for protons and pions is applied only below 5 GeV/c of the electron momentum at the inner wall of the TPC, while above 5 GeV/c the rejection is not applied to avoid reductions in the electron reconstruction efficiency. J/ψ candidates are then obtained by considering all opposite-sign charged electron pairs. In 0–10% most central collisions, only candidates where both electron decay tracks have a hit in the first layer of the SPD are considered to optimise both the spatial resolution and signal-to-background ratio. For other centrality classes as well as in the highest p_{T} interval (7–10 GeV/c) in the 0–10% centrality class, where the signal-to-background ratio is better, the condition is released to increase the efficiency. Pair candidates where neither of the decay products has a hit in the first layer of the SPD are excluded due to the poor resolution of the secondary vertex.

Separation of prompt and non-prompt J/ψ. The measurement of the non-prompt J/ψ fraction is obtained through an unbinned two-dimensional likelihood fit procedure applied to reconstructed J/ψ candidate pairs, following the same techniques employed in previous publications [53, 54, 65–67]. A simultaneous unbinned log-likelihood fit of the J/ψ candidate distribution as a function of invariant mass (m_{ee}) and pseudoproper decay length (x) values is performed. The pseudoproper decay length is defined as $x = c \times L_{\mathrm{xy}} \times m_{\mathrm{J}/\psi}/p_{\mathrm{T}}$, where $L_{\mathrm{xy}} = (\vec{L} \times \vec{p_{\mathrm{T}}})/p_{\mathrm{T}}$ represents the projection in the transverse plane of the vector pointing from the primary vertex to the J/ψ decay vertex ($\vec{L}$) and $m_{\mathrm{J}/\psi}$ is the J/ψ mass provided by the Particle Data Group (PDG) [68]. The fit procedure maximises the logarithm of a likelihood function

$$\ln \mathcal{L} = \sum_{i=1}^{N} \ln \Big[f_{\mathrm{Sig}} \times F_{\mathrm{Sig}}(x^i) \times M_{\mathrm{Sig}}(m^i_{\mathrm{ee}}) + (1 - f_{\mathrm{Sig}}) \times F_{\mathrm{Bkg}}(x^i) \times M_{\mathrm{Bkg}}(m^i_{\mathrm{ee}}) \Big], \tag{3.2}$$

where N is the number of J/ψ candidates within the invariant mass interval $2.72 < m_{\mathrm{ee}} < 3.40\,\mathrm{GeV}/c^2$ ($2.60 < m_{\mathrm{ee}} < 3.60\,\mathrm{GeV}/c^2$) in the centrality interval 0–10% (10–90%). A tighter invariant mass window is considered in most central collisions in order to increase the signal-to-background ratio in the fitting region, but still with a large enough sample of candidates to constrain the background probability density functions (PDFs). The relative amount of signal candidates, both prompt and non-prompt J/ψ, with respect to the total number of candidates is quantified by the fit parameter f_{Sig}. The PDFs entering in eq. (3.2), namely $F_{\mathrm{Sig}}(x)$ and $F_{\mathrm{Bkg}}(x)$ ($M_{\mathrm{Sig}}(x)$ and $M_{\mathrm{Bkg}}(x)$), are used to describe the pseudoproper decay length (invariant mass) distributions of signal and background, respectively. The pseudoproper decay length PDF of the signal is defined as

$$F_{\mathrm{Sig}}(x) = f'_{\mathrm{B}} \times F_{\mathrm{B}}(x) + (1 - f'_{\mathrm{B}}) \times F_{\mathrm{prompt}}(x), \tag{3.3}$$

JHEP02(2024)066

where $F_{\mathrm{B}}(x)$ and $F_{\mathrm{prompt}}(x)$ are the x PDFs for non-prompt and prompt J/ψ, respectively, while f'_{B} represents the fraction of J/ψ originating from beauty-hadron decays in the sample of selected dielectron candidates. Both f'_{B} and f_{Sig} are left as free parameters in the fitting procedure. A correction to the f'_{B} fraction obtained from the fit is applied to take into account the different average acceptance-times-efficiencies of prompt and non-prompt J/ψ, which is a consequence of two effects: *(i)* different J/ψ p_{T} distributions inside the wide p_{T} intervals where the measurements are provided; *(ii)* different J/ψ polarisation, which can modify angular distributions of decay products and thus the J/ψ acceptance. The corrected fraction of non-prompt J/ψ, f_{B}, is obtained as

$$f_{\mathrm{B}} = \left(1 + \frac{1 - f'_{\mathrm{B}}}{f'_{\mathrm{B}}} \times \frac{\langle A \times \epsilon \rangle_{\mathrm{B}}}{\langle A \times \epsilon \rangle_{\mathrm{prompt}}}\right)^{-1}, \tag{3.4}$$

where $\langle A \times \epsilon \rangle_{\mathrm{prompt}}$ and $\langle A \times \epsilon \rangle_{\mathrm{B}}$ represent the average acceptance-times-efficiency values for prompt and non-prompt J/ψ, respectively, in the considered p_{T} interval. The functional forms of the different PDFs in eq. (3.2) are determined either based on data or on Monte Carlo (MC) simulations, and are computed using the same procedures as in previous analyses [53, 54, 65, 66]. The PDFs corresponding to the signal component, namely $F_{\mathrm{prompt}}(x)$, $F_{\mathrm{B}}(x)$, and $M_{\mathrm{Sig}}(m_{\mathrm{ee}})$, as well as acceptance-times-efficiency corrections of prompt and non-prompt J/ψ in eq. (3.4), are determined from MC simulations. These simulations consist of prompt and non-prompt J/ψ meson signals embedded in a background sample of Pb–Pb collisions at $\sqrt{s_{\mathrm{NN}}} = 5.02\,\mathrm{TeV}$ produced with HIJING [69]. The intervals of centrality for the Pb–Pb collisions considered in MC simulations are the same as those selected in experimental data. The prompt J/ψ component is simulated with a p_{T} spectrum based on existing inclusive J/ψ Pb–Pb measurements at midrapidity, while PYTHIA 6.4 [70] is used to generate beauty hadrons for non-prompt J/ψ simulations. The decays of beauty hadrons into final states containing a J/ψ meson are handled by the EvtGen R01-03-00 [71] package, while the J/ψ decay into the dielectron channel is performed using the EvtGen package coupled with the PHOTOS model [72] for the treatment of radiative decays (J/$\psi \rightarrow \mathrm{e^+e^-}\gamma$). Prompt J/$\psi$ are assumed to be unpolarised, while for the non-prompt J/ψ a small residual polarisation as predicted by EvtGen [71] is considered. No further assumptions on the polarisation of both components are accounted, considering that existing measurements indicate small or no polarisation [73, 74]. The particle transport through the ALICE apparatus is handled by GEANT3 [75], considering a detailed description of the detector material and geometry. Detector responses and calibrations in MC simulations are tuned to data, taking into account time-dependent running conditions of all detectors included in the data acquisition.

The p_{T} spectrum of prompt J/ψ in simulations is tuned to match experimentally observed distributions, taking into account the centrality dependence. In particular, the fits to measured inclusive J/ψ yields from earlier publications [28, 31] are considered. To propagate the associated experimental uncertainties to the systematic uncertainties on acceptance-times-efficiency, all possible variations of the p_{T} shape within the envelope obtained by varying the fitting parameters according to their uncertainties are also considered. For non-prompt J/ψ, different hypotheses are considered for the p_{T} distributions, including or excluding shadowing or suppression effects predicted by model calculations, such as those discussed in section 4.

JHEP02(2024)066

Centrality class	m_{ee} sidebands (GeV/c^2)	p_T intervals (GeV/c)
0–10%	2.72−2.8, 2.8−2.9, 3.2−3.3, 3.3−3.4	1.5−3, 3−5, 5−7, 7−10
10–30%, 30–50%, 50–90%	2.64−2.75, 2.75−2.85, 3.2−3.35, 3.35−3.52	1.5−3, 3−5, 5−10

Table 1. Invariant mass and p_T intervals considered for the definition of $F_{Bkg}(x)$ in different centrality classes (see text for details).

Taking into account all hypotheses discussed above for prompt and non-prompt J/ψ p_T spectra, an average correction factor for f'_B is evaluated. As the acceptance-times-efficiency corrections are weakly dependent on p_T, the resulting correction applied on f'_B according to eq. (3.4) is small, being ∼5% for the p_T integrated case, while for the different p_T intervals it ranges between 1% to 3%, depending on the width of the interval.

The resolution function, $F_{prompt}(x)$ in eq. (3.3), defines the accuracy of x in the reconstruction, and affects all different PDFs related to the pseudoproper decay length. It is described by the sum of two Gaussians and a symmetric power law function. It is determined as a function of both p_T and centrality from MC simulations. A tuning procedure is applied in MC simulations to minimise the residual discrepancy with respect to data in the average distance of closest approach (DCA) of the track to the reconstructed interaction vertex in a plane perpendicular to the beam direction. A small centrality dependence is found for the x resolution, in particular the RMS of the resolution function changes by about 5% across different centrality classes, getting worse towards more central collisions. For the non-prompt J/ψ, the pseudoproper decay length distribution $F_B(x)$ is modelled by the kinematic distribution of J/ψ from beauty-hadron decays obtained from the MC simulation described above, and convoluted with the resolution function. Finally, MC simulations are also employed to determine the shape of the invariant mass signal $M_{Sig}(m_{ee})$, which is parametrised using a Crystal Ball function [76]. Background PDFs, for both invariant mass and pseudoproper decay length distributions, are built from data. The invariant mass background shape $M_{Bkg}(m_{ee})$, parametrised by a third order polynomial function, is estimated using the event-mixing technique, already used for the inclusive J/ψ analysis at midrapidity [31], which also takes into account the residual background originating from correlated semileptonic decays of heavy-flavour hadrons. For the pseudoproper decay length background function, $F_{Bkg}(x)$, the same functional form and strategy described in ref. [54] is used. The function is determined for each centrality class by a fit to the data in four invariant mass regions on the sidebands of the J/ψ mass peak and in different p_T intervals, as summarised in table 1. In each p_T interval, the x background function in the invariant mass region which contains the nominal J/ψ mass value is obtained by an interpolation procedure as the weighted combination of the PDFs determined in the other four invariant mass regions. The weights are chosen inversely proportional to the absolute or squared difference between the mean of the invariant mass distribution in the given mass interval and that in the interpolated region. Both hypotheses for the weights are considered for the study of the systematic uncertainty on the pseudoproper decay length background PDF. Additionally, the internal edges that define the invariant mass windows in table 1 are shifted by ± 20 MeV/c^2, either in the same or opposite directions, and the interpolation procedure inside the signal region is repeated. For each p_T interval,

JHEP02(2024)066

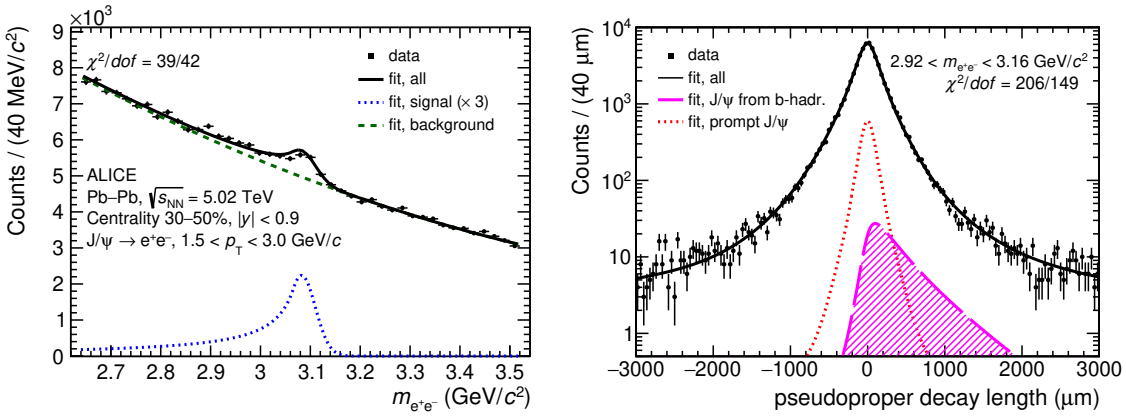

Figure 1. Invariant mass (left panel) and pseudoproper decay length (right panel) distributions of J/ψ candidates with maximum likelihood fit projections superimposed. The distributions in the figures correspond to selected candidates with $1.5 < p_{\mathrm{T}} < 3.0\,\mathrm{GeV}/c$ in the centrality class 30–50%. The pseudoproper decay length distribution is shown for J/ψ candidates reconstructed under the J/ψ mass peak, i.e. for $2.92 < m_{\mathrm{ee}} < 3.16\,\mathrm{GeV}/c^2$, for display purposes only. The χ^2 values, obtained by comparing the binned distributions of data points and the corresponding projections of the total fit function, are also reported.

a total of 9 (variations of mass intervals) × 2 (linear or quadratic weights) = 18 attempts are obtained for $F_{\mathrm{Bkg}}(x)$, which are used in turn in the unbinned likelihood fit procedure to determine f'_{B}. As the choice of a specific definition of mass intervals is in principle arbitrary, the central value of f'_{B} is computed considering the average of all the different attempts. Figure 1 shows an example of invariant mass (left panel) and pseudoproper decay length (right panel) distributions, corresponding to the centrality class 30–50% and transverse momentum range $1.5 < p_{\mathrm{T}} < 3.0\,\mathrm{GeV}/c$, with superimposed projections of the total maximum likelihood fit functions. The non-prompt J/ψ fraction is measured in four (three) p_{T} intervals in the centrality class 0–10% (10–30% and 30–50%), as well as in the p_{T} integrated case ($1.5 < p_{\mathrm{T}} < 10\,\mathrm{GeV}/c$) in the centrality classes 0–10%, 10–30%, 30–50%, and 50–90%.

Systematic uncertainties. The systematic uncertainties on the measured non-prompt J/ψ fractions in different p_{T} intervals and centrality classes are summarised in table 2. Most of the contributions are due to the incomplete knowledge of the different PDFs of m_{ee} and x in the likelihood fit. An additional contribution originates from the assumptions of the p_{T} distributions of J/ψ in MC simulations.

The dominant uncertainty is represented by the PDF of the pseudoproper decay length background, especially towards low p_{T} and more central collisions. Other contributions which become dominant in some cases are those originating from the resolution function, in particular in the lowest p_{T} intervals of each centrality, and the assumptions of the p_{T} distributions of J/ψ used in simulations, the latter particularly relevant for the p_{T} integrated case.

The uncertainty on the resolution function is computed by considering the residual mismatch between data and MC simulations observed on the single track DCA resolution after the tuning procedure. The RMS of the resolution function is changed accordingly and

JHEP02(2024)066

	Cent. 0–10%			Cent. 10–30%			Cent. 30–50%			Cent. 50–90%
p_{T} (GeV/c)	1.5–10	1.5–3	7–10	1.5–10	1.5–3	5–10	1.5–10	1.5–3	5–10	1.5–10
Resolution function	2.5	5.0	1.0	3.5	5.0	1.0	2.5	3.5	1.0	2.5
x PDF of background	11.0	15.0	5.0	6.0	14.0	5.0	5.0	8.0	3.0	4.0
MC p_{T} distribution	6.0	1.5	3.0	6.0	1.5	4.0	6.0	1.5	3.0	6.0
x PDF of non-prompt J/ψ	2.0	2.0	1.5	2.0	4.0	1.0	2.0	2.5	1.0	3.0
m_{ee} PDF of signal	0.5	1.5	0.5	0.5	0.5	0.5	0.5	0.5	0.5	0.5
m_{ee} PDF of background	0.5	2.5	0.5	1.0	2.5	0.5	0.5	1.5	0.5	0.5
Total	13.0	16.3	6.1	9.6	15.3	6.6	8.5	9.3	4.5	8.2

Table 2. Systematic uncertainties on f_{B}, expressed in %, for the p_{T} integrated case, as well as for the lowest and the highest p_{T} interval in each centrality class.

the relative variation on f_{B} is taken as systematic uncertainty. The corresponding values are found to be larger at low p_{T} due to the worse pseudoproper decay length resolution and weakly dependent on centrality.

The uncertainty due to the pseudoproper decay length background PDF is estimated by computing the RMS of non-prompt J/ψ fraction values obtained after changing the $F_{\mathrm{Bkg}}(x)$ in the likelihood fit, considering the eighteen attempts previously mentioned, which depend on the choice of the m_{ee} sidebands. The uncertainty on f_{B} due to the $F_{\mathrm{Bkg}}(x)$ is the major contribution, especially at low-p_{T} and more central collisions where the signal-to-background ratio gets worse.

The systematic uncertainty related to the p_{T} distributions of prompt and non-prompt J/ψ mesons in MC simulations, mainly affecting the acceptance-times-efficiency correction on f_{B} according to eq. (3.4), is evaluated by varying the prompt and non-prompt J/ψ p_{T} shape considering the variations previously discussed in this section. Taking into account all combinations, an average correction factor for f'_{B} is evaluated, while the maximum variation with respect to the average value is used to estimate the corresponding systematic uncertainty. This contribution increases for wider p_{T} intervals, reaching about 6% for the p_{T} integrated interval, and is relatively independent of centrality.

To quantify the systematic uncertainty related to the shape of the x PDF of non-prompt J/ψ, the p_{T} distribution of non-prompt J/ψ is changed according to the same hypotheses considered for the estimate of the systematic uncertainty on the $\langle A \times \epsilon \rangle$ correction on f_{B}. Furthermore, the systematic uncertainty of the non-prompt J/ψ x PDF originating from the description of the $h_{\mathrm{b}} \to \mathrm{J}/\psi + \mathrm{X}$ decay kinematic, with h_{b} representing any beauty mesons or baryons, is evaluated by considering PYTHIA 6.4 instead of EvtGen for decaying beauty hadrons. For both EvtGen and PYTHIA, all default decay modes of beauty hadrons available in the corresponding package and including a J/ψ in the final state, are considered.

The uncertainty on the invariant mass PDF of the J/ψ signal is evaluated by changing the width of the Crystal Ball function in order to vary the fraction of candidates within the signal interval $2.92 < m_{\mathrm{ee}} < 3.16\,\mathrm{GeV}/c^2$ by $\pm$ 2.5%. The latter variation corresponds to the systematic uncertainty on the MC signal shape assigned in the inclusive J/ψ analysis [31].

The uncertainty related to the invariant mass background PDF is evaluated by taking the maximum variation obtained for f_{B} after using in the likelihood fit procedure alternative

JHEP02(2024)066

p_{T} (GeV/c)	$f_{\mathrm{B}}^{\mathrm{pp}}$ at $\sqrt{s}$ = 5.02 TeV
1.5–10	0.183 ± 0.004
1.5–3	0.110 ± 0.007
3–5	0.142 ± 0.004
5–7	0.190 ± 0.003
7–10	0.257 ± 0.005
5–10	0.227 ± 0.004

Table 3. Fraction of non-prompt J/ψ with the corresponding uncertainties in pp collisions at $\sqrt{s}$ = 5.02 TeV, obtained through the interpolation procedure, in different p_{T} intervals (see text for details).

functions, namely fourth and fifth order polynomial functions, for fitting the event mixing based distribution used for the determination of $M_{\mathrm{Bkg}}(x)$.

The overall systematic uncertainty on f_{B} reaches a maximum of about 16% in the lowest p_{T} interval and in 0–10% centrality class, mostly as a consequence of both the increasing combinatorial background in more central collisions and the worsening of the x resolution at low transverse momenta.

3.2 Non-prompt J/ψ fractions in pp collisions at $\sqrt{s}$ = 5.02 TeV

In pp collisions at $\sqrt{s}$ = 5.02 TeV, non-prompt J/ψ fractions are measured at midrapidity by the ALICE collaboration [67] down to p_{T} = 2 GeV/c. However, as the corresponding uncertainties are large and the p_{T} intervals in pp collisions do not match those of the Pb–Pb measurements, the p_{T}-differential f_{B} fractions are obtained via an interpolation procedure, already used in previous p–Pb and Pb–Pb analyses [53, 54, 65, 66]. This procedure is based on available non-prompt J/ψ fraction measurements in pp and p$\overline{\mathrm{p}}$ collisions at midrapidity at several centre-of-mass energies, namely $\sqrt{s}$ = 1.96 TeV (CDF [77]), 5.02 TeV (ALICE [67], CMS [78]), 7 TeV (ALICE [79], ATLAS [80, 81], CMS [82]) and 8 TeV (ATLAS [80]). In particular, using the semi-phenomenological function described in ref. [54], which employs FONLL to describe the non-prompt J/ψ production cross section, the non-prompt J/ψ fraction in pp collisions at $\sqrt{s}$ = 5.02 TeV ($f_{\mathrm{B}}^{\mathrm{pp}}$) as a function of p_{T}, needed for the computation of the reference for prompt and non-prompt J/ψ R_{AA} measurements, is derived via an energy interpolation. The average $f_{\mathrm{B}}^{\mathrm{pp}}$ in each p_{T} interval considered in the Pb–Pb analysis is obtained by reweighting the p_{T}-differential $f_{\mathrm{B}}^{\mathrm{pp}}$ values by the inclusive p_{T}-differential J/ψ cross section in pp collisions at $\sqrt{s}$ = 5.02 TeV [83].

The values of $f_{\mathrm{B}}^{\mathrm{pp}}$ in the p_{T} intervals considered in the Pb–Pb analysis are summarised in table 3. The uncertainty, which amounts to about 6.5% in the lowest p_{T} interval and decreases to about 1.5% at higher p_{T}, includes the contribution from experimental data and FONLL predictions, as well as the systematic uncertainty due to the choice of the functional form assumed for the energy interpolation (namely linear, exponential, and power law function).

JHEP02(2024)066

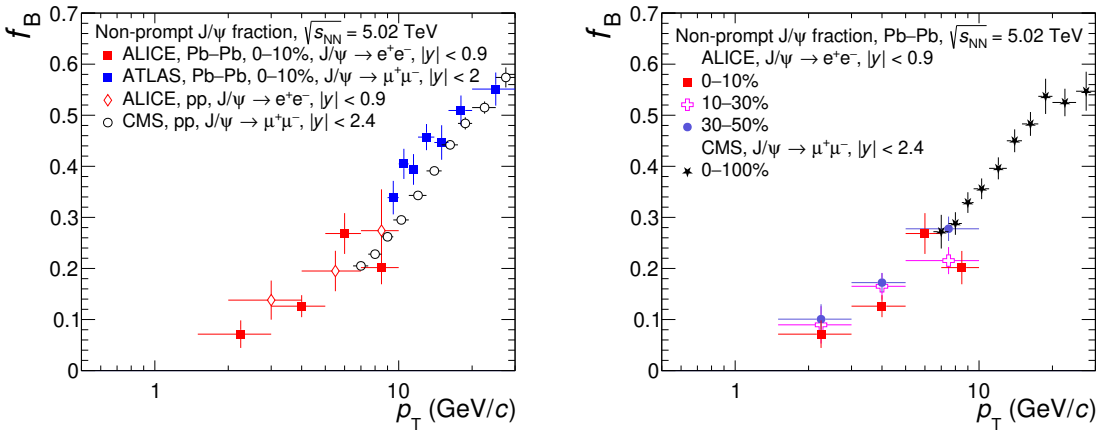

Figure 2. Non-prompt J/ψ fraction as a function of transverse momentum measured by the ALICE collaboration in 0–10% most central Pb–Pb collisions (left panel) and in all centrality classes (right panel). Results in the left panel are compared with ATLAS midrapidity measurements [29] in the centrality class 0–10%, and with ALICE [67] and CMS [30] measurements in pp collisions at $\sqrt{s}$ = 5.02 TeV. The ALICE measurements in the right panel are compared with similar midrapidity measurements from CMS [30], performed in the centrality class 0–100%. In both panels, the error bars represent the quadratic sum of statistical and systematic uncertainties.

4 Results and discussion

4.1 Non-prompt J/ψ fractions and J/ψ yields

The non-prompt J/ψ fraction measured by the ALICE collaboration in 0–10% Pb–Pb collisions as a function of p_{T} in $|y| < 0.9$ is shown in the left hand panel of figure 2. It is compared with similar results obtained by the ATLAS collaboration [29] at midrapidity, and available for p_{T} above 9.5 GeV/c. In the right hand panel, the p_{T}-differential non-prompt J/ψ fractions measured by the ALICE collaboration in different centrality classes are compared with CMS results [30] available for $p_{\mathrm{T}} > 6.5$ GeV/c in the centrality class 0–100%. The ALICE results complement the existing high-p_{T} measurements from ATLAS and CMS, matching the decreasing trend observed from high towards low p_{T}. The results in the centrality interval 0–10% suggest a smaller f_{B} compared to other centralities, in particular at low transverse momentum. In the left panel, non-prompt J/ψ fraction measurements in pp collisions at $\sqrt{s} = 5.02$ TeV obtained by the ALICE [67] and CMS [30] collaborations are also shown for comparison, and exhibit a trend similar to the one observed in Pb–Pb collisions. In the p_{T} range 10 to 20 GeV/c, the non-prompt J/ψ fractions are clearly higher in Pb–Pb compared to pp collisions, possibly suggesting a stronger nuclear suppression of prompt charmonia compared to beauty hadrons. On the other hand, at low-p_{T} results in the two systems exhibit similar values within uncertainties.

Figure 3 presents the non-prompt J/ψ fraction as a function of centrality, expressed in terms of the average number of participants $\langle N_{\mathrm{part}} \rangle$, measured by ALICE in Pb–Pb collisions at $\sqrt{s_{\mathrm{NN}}} = 5.02$ TeV in the transverse momentum interval $1.5 < p_{\mathrm{T}} < 10$ GeV/c. Within uncertainties, no centrality dependence is observed between peripheral and semicentral collisions, while the measured f_{B} in 0–10% most central collisions decreases in comparison

JHEP02(2024)066

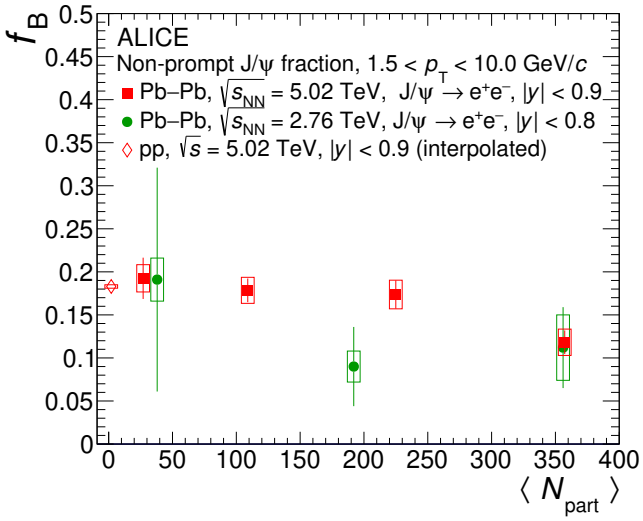

Figure 3. Centrality dependence (expressed in terms of average number of participants) of the non-prompt J/ψ fraction measured by ALICE in Pb–Pb collisions at $\sqrt{s_{NN}} = 5.02$ TeV in the transverse momentum interval $1.5 < p_T < 10$ GeV/c. Results are compared with previous ALICE measurements performed in Pb–Pb collisions at $\sqrt{s_{NN}} = 2.76$ TeV [54]. The p_T-integrated non-prompt J/ψ fraction in pp collisions at $\sqrt{s} = 5.02$ TeV obtained from an interpolation procedure (see text for details) is also shown. Statistical and systematic uncertainties are shown by error bars and boxes, respectively.

to an average value computed by considering all other centralities with a significance of about 2.5σ considering both statistical and systematic uncertainties. This is consistent with the observations for the p_T-dependent results shown in figure 2 and is compatible with the hypothesis of a strong contribution of prompt J/ψ originating from regeneration, which is expected to be larger in central compared to peripheral collisions. Current results are compared with earlier ALICE measurements based on Pb–Pb collisions at $\sqrt{s_{NN}}$ =2.76 TeV [54]. The statistical precision is significantly improved thanks to the larger event sample available from LHC Run 2. In the same figure, the p_T-integrated non-prompt J/ψ fraction in pp collisions at $\sqrt{s} = 5.02$ TeV obtained by the interpolation procedure described in section 3.2 is also shown. The corresponding value is found to be comparable with the non-prompt J/ψ fractions measured in peripheral and semicentral Pb–Pb collisions.

The p_T-differential production yields of prompt and non-prompt J/ψ in a given centrality interval are computed by combining the non-prompt J/ψ fractions with the measured yields of inclusive J/ψ [31], $\mathrm{d}N^{\text{incl. J}/\psi}/\mathrm{d}y\mathrm{d}p_T$, as

$$\frac{\mathrm{d}N^{\mathrm{J}/\psi\leftarrow \mathrm{h_B}}}{\mathrm{d}y\mathrm{d}p_T} = f_B \times \frac{\mathrm{d}N^{\text{incl. J}/\psi}}{\mathrm{d}y\mathrm{d}p_T}, \qquad \frac{\mathrm{d}N^{\text{prompt J}/\psi}}{\mathrm{d}y\mathrm{d}p_T} = (1 - f_B) \times \frac{\mathrm{d}N^{\text{incl. J}/\psi}}{\mathrm{d}y\mathrm{d}p_T}. \tag{4.1}$$

Figure 4 shows the p_T-differential production yields of prompt and non-prompt J/ψ in the centrality interval 0–10%. Statistical and systematic uncertainties on prompt and non-prompt J/ψ yields are evaluated by adding in quadrature the corresponding uncertainties on f_B and inclusive J/ψ yields, the latter discussed in detail in ref. [31]. The statistical uncertainties of inclusive J/ψ yields vary from about 5% to 10%, depending on the p_T and the centrality of the collision. Regarding the systematic uncertainty of the inclusive J/ψ yield, it ranges

JHEP02(2024)066

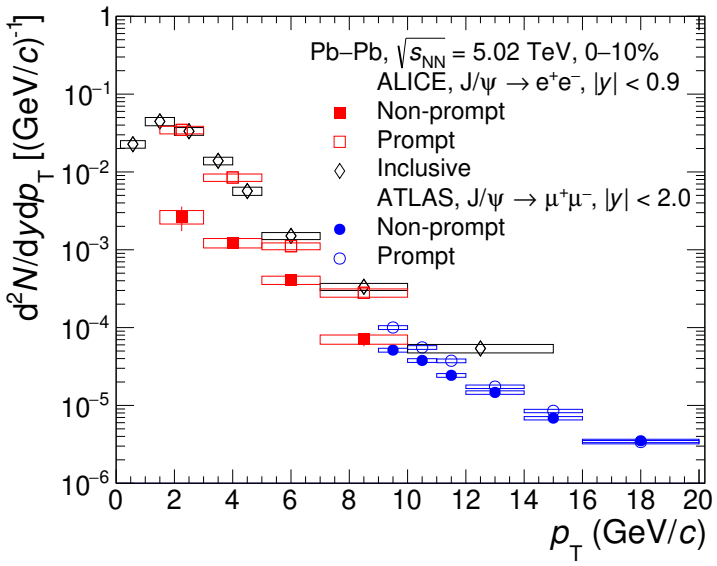

Figure 4. Prompt and non-prompt J/ψ p_{T}-differential production yields measured by ALICE in the 0–10% centrality class at midrapidity, compared with similar measurements from the ATLAS collaboration [29] in the same centrality class. Inclusive J/ψ yields measured by the ALICE collaboration in 0–10% [31] are shown for comparison. Error bars and boxes represent statistical and systematic uncertainties, respectively.

within 10–12% (8–10%) in the centrality class 0–10% (30–50%) and shows no significant p_{T} dependence. The measurements from ALICE are compared with p_{T}-differential production yields obtained by the ATLAS collaboration [29], as well as with inclusive J/ψ measurements performed by the ALICE collaboration [31]. As already observed for the non-prompt J/ψ fraction, the ALICE measurements provide complementary p_{T} coverage to ATLAS results, and they extend the measurement down to $p_{\mathrm{T}} = 1.5\,\mathrm{GeV}/c$. In addition, the ALICE and ATLAS results are qualitatively compatible in the overlapping region and show similar slopes, which result in an overall smooth trend over the full p_{T} range. Given the relatively small non-prompt J/ψ fraction below $10\,\mathrm{GeV}/c$, the inclusive J/ψ yield and that of the prompt J/ψ, both measured by the ALICE collaboration, are found to be comparable. However, the inclusive J/ψ yield is measured in finer p_{T} intervals and subtends a wider range in p_{T}.

4.2 J/ψ nuclear modification factors

The nuclear modification factor R_{AA} of prompt and non-prompt J/ψ is obtained by combining the R_{AA} of inclusive J/ψ [31], with the non-prompt J/ψ fractions measured in Pb–Pb collisions at $\sqrt{s_{\mathrm{NN}}} = 5.02\,\mathrm{TeV}$ normalised to those in pp collisions obtained at the same centre-of-mass energy through the interpolation procedure described in section 3.2:

$$R_{\mathrm{AA}}^{\mathrm{J/\psi \leftarrow h_B}} = \frac{f_{\mathrm{B}}^{\mathrm{Pb-Pb}}}{f_{\mathrm{B}}^{\mathrm{pp}}} \times R_{\mathrm{AA}}^{\text{inclusive J/}\psi}, \qquad R_{\mathrm{AA}}^{\text{prompt J/}\psi} = \frac{1 - f_{\mathrm{B}}^{\mathrm{Pb-Pb}}}{1 - f_{\mathrm{B}}^{\mathrm{pp}}} \times R_{\mathrm{AA}}^{\text{inclusive J/}\psi}. \quad (4.2)$$

Statistical and systematic uncertainties on prompt and non-prompt J/ψ R_{AA} are obtained by adding in quadrature the corresponding uncertainties on inclusive J/ψ R_{AA} [31] and non-prompt J/ψ fractions in Pb–Pb and in pp collisions, assuming all of them uncorrelated

JHEP02(2024)066

from each other. Uncertainties on inclusive J/ψ $R_{\rm AA}$, both statistical and systematic, include the corresponding contributions due to inclusive J/ψ yields previously mentioned and inclusive J/ψ cross section in pp collisions at $\sqrt{s}$ = 5.02 TeV [83], the latter used as reference in the inclusive J/ψ $R_{\rm AA}$ computation. The statistical uncertainty on the pp reference cross section increases with $p_{\rm T}$ from about 7% to 18%, while the systematic uncertainty is poorly dependent on $p_{\rm T}$ and it amounts to about 6%. The latter value do not include the normalisation uncertainty due to luminosity determination, which is 2.2% and it is considered within the global uncertainties when computing $R_{\rm AA}$.

The $p_{\rm T}$-differential nuclear modification factor of prompt J/ψ is shown in figure 5 in different centrality classes, namely 0–10% (top left panel), 10–30% (top right panel) and 30–50% (bottom left panel). Global uncertainties, shown as boxes around unity, include correlated uncertainties on the pp reference due to normalisation as well as on the $\langle T_{\rm AA}\rangle$ [31]. The latter uncertainty decreases with the collision centrality, varying from 0.7% in 0–10% most central collisions to 2% in the 50–90% centrality class. The $R_{\rm AA}$ of prompt J/ψ in $1.5 < p_{\rm T} < 10\,{\rm GeV}/c$ and as a function of centrality is shown in the bottom right panel of the same figure. The global uncertainty includes the contributions from the inclusive J/ψ cross section and from $f_{\rm B}^{\rm pp}$ in pp collisions, both integrated over $p_{\rm T}$ ($1.5 < p_{\rm T} < 10\,{\rm GeV}/c$). For $p_{\rm T} > 5\,{\rm GeV}/c$, the prompt J/$\psi$ $R_{\rm AA}$ in the centrality classes 10–30% and 30–50% reaches a value of about 0.4, while in 0–10% collisions it decreases to about 0.2, indicating a stronger suppression. The prompt J/ψ $R_{\rm AA}$ increases towards low $p_{\rm T}$ and it exceeds unity in the lowest $p_{\rm T}$ interval (1.5–3 GeV/c) of the 0–10% most central collisions. As a consequence, the $p_{\rm T}$ integrated prompt J/ψ $R_{\rm AA}$ ($1.5 < p_{\rm T} < 10\,{\rm GeV}/c$) also rises towards most central collisions, as shown in the bottom right panel of figure 5. According to prompt J/ψ measurements performed by the ALICE collaboration in p–Pb collisions at $\sqrt{s_{\rm NN}} = 5.02$ TeV [53], the $R_{\rm pPb}$ is found to be lower than unity within $1 < p_{\rm T} < 3\,{\rm GeV}/c$, suggesting significant CNM effects at play in Pb–Pb collisions in this transverse momentum region, while it becomes compatible with unity for $p_{\rm T} > 3\,{\rm GeV}/c$. The results from the ALICE collaboration are compared with similar measurements carried out by the ATLAS [29] and CMS [30] collaborations in the rapidity intervals $|y| < 2.0$ and $|y| < 2.4$, respectively. In the centrality interval 0–10%, the results from CMS and ATLAS are in good agreement with the ALICE measurements in the overlapping $p_{\rm T}$ interval, while in semicentral collisions the agreement is better with CMS than with ATLAS. It is worth noting that a smaller suppression for ATLAS measurements is expected in semicentral events, as the corresponding results use a significantly more peripheral collision sample compared to ALICE and CMS.

Figure 6 shows the nuclear modification factor of non-prompt J/ψ as a function of $p_{\rm T}$ in the same centrality classes discussed previously for the prompt J/ψ $R_{\rm AA}$, namely 0–10%, 10–30% and 30–50%. The boxes around unity represent global uncertainties due to the normalisation of the pp reference cross section and $\langle T_{\rm AA}\rangle$. Unlike the prompt J/$\psi$ $R_{\rm AA}$, the $p_{\rm T}$-differential nuclear modification factors of non-prompt J/ψ are similar in the different centrality classes within experimental uncertainties below $5\,{\rm GeV}/c$, while at higher $p_{\rm T}$ the suppression is larger in 0–10% most central collisions. The $p_{\rm T}$-integrated $R_{\rm AA}$ in the bottom right panel of figure 6 hints at a decreasing trend towards more central collisions, reaching an $R_{\rm AA}$ value of about 0.6 in the 0–10% centrality class. In the case of non-prompt J/ψ,

JHEP02(2024)066

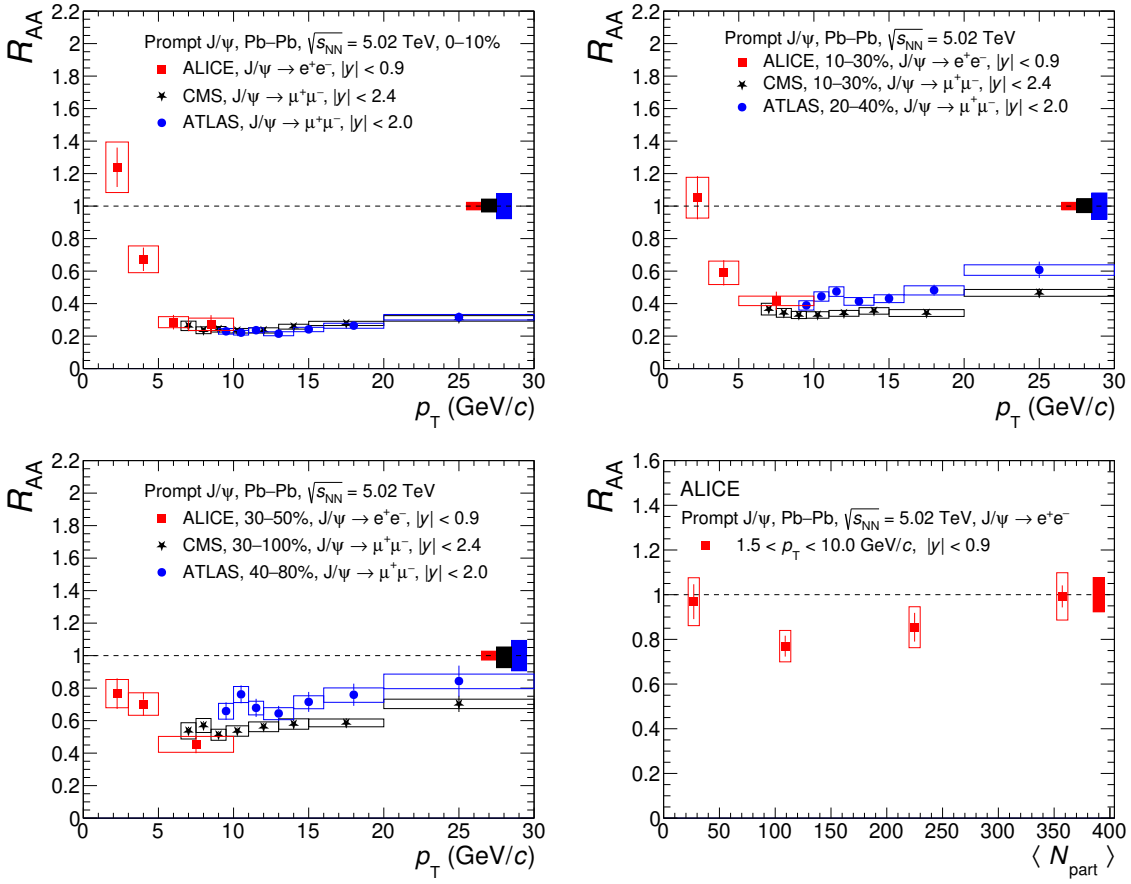

Figure 5. Nuclear modification factor of prompt J/ψ as a function of p_{T} in 0–10% (upper left panel), 10–30% (top right panel) and 30–50% (bottom left panel) centrality classes. Results are compared with similar measurements from the ATLAS [29] and CMS [30] collaborations. The centrality dependent prompt J/ψ R_{AA} in $1.5 < p_{\mathrm{T}} < 10\,\mathrm{GeV}/c$ is shown in the bottom right panel (centrality is expressed in terms of average number of participants). Error bars and boxes represent, respectively, statistical and systematic uncertainties uncorrelated with p_{T} (centrality, for the bottom right panel). Global uncertainties are shown as boxes around unity.

CNM effects are found to be small in the full measured p_{T} interval, as non-prompt J/ψ R_{pPb} measurements at $\sqrt{s_{\mathrm{NN}}} = 5.02\,\mathrm{TeV}$ [53] are everywhere compatible with unity, although uncertainties are large. Therefore, the observed modification can be attributed to the QGP formation in Pb–Pb collisions. Results as a function of p_{T} are shown together with non-prompt J/ψ R_{AA} measurements from the ATLAS [29] and CMS [30] collaborations, which are in good agreement with ALICE measurements in the overlapping p_{T} region. In 0–10% most central collisions, the R_{AA} from ALICE in the highest p_{T} interval shows a small tension of about 1.4σ and 2.5σ with respect to ATLAS and CMS, respectively. The non-prompt J/ψ R_{AA} measurements in 0–10% and 30–50% centrality classes are also compared with non-prompt D^0 results [84] measured at midrapidity by the ALICE collaboration. The results are compatible within uncertainties, despite possible differences that might originate from different decay kinematics of beauty hadrons to J/ψ and D^0.

JHEP02(2024)066

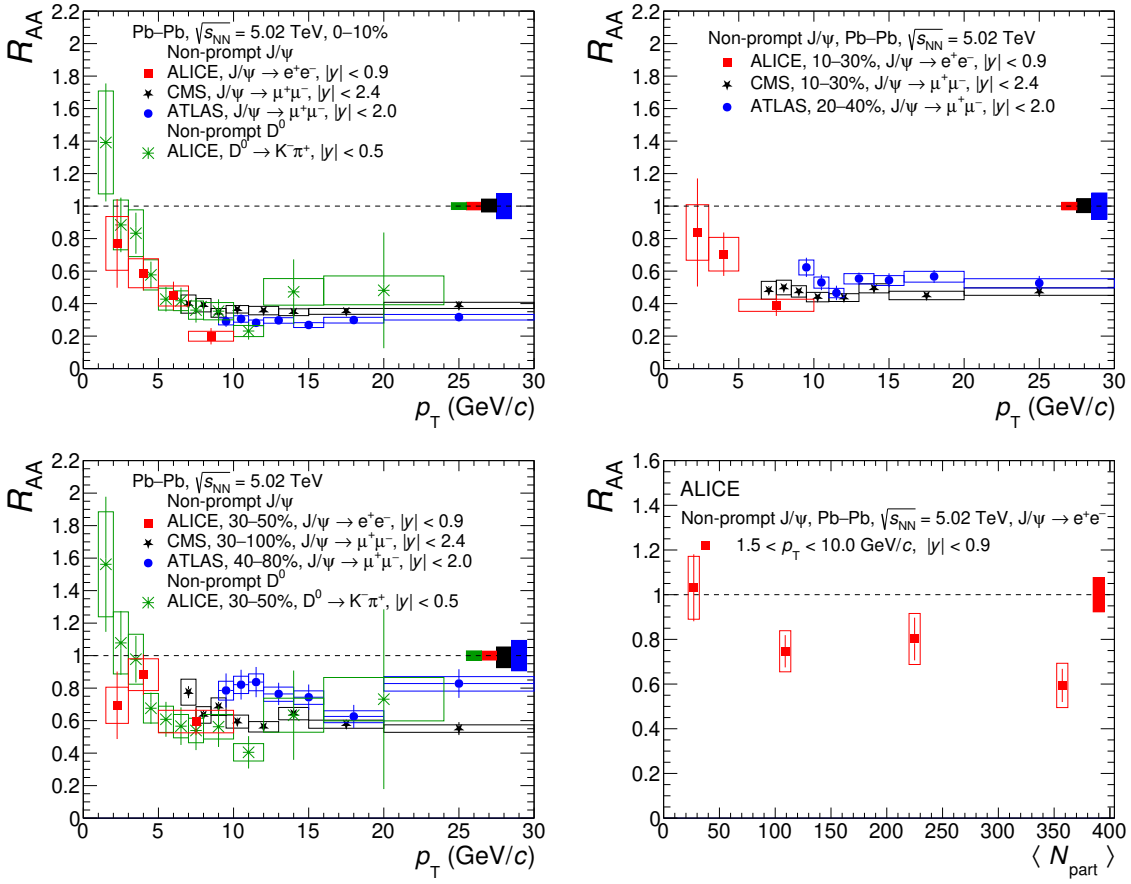

Figure 6. Nuclear modification factor of non-prompt J/ψ as a function of p_{T} in the 0–10% (upper left panel), 10–30% (top right panel) and 30–50% (bottom left panel). Results are compared with similar measurements from the ATLAS [29] and CMS [30] collaborations. Results in 0–10% and 30–50% are also compared to non-prompt D^0 R_{AA} measurements [84] in the same centrality classes. The centrality dependent non-prompt J/ψ R_{AA} in $1.5 < p_{\mathrm{T}} < 10\,\mathrm{GeV}/c$ is shown in the bottom right panel (centrality is expressed in terms of average number of participants). Error bars and boxes represent statistical and systematic uncertainties uncorrelated with p_{T} (centrality, for the bottom right panel). Global uncertainties are shown as boxes around unity.

4.3 Comparison with models for prompt J/ψ production

In the following, prompt J/ψ measurements are compared with different phenomenological models in relativistic heavy-ion collisions.

Figure 7 shows the p_{T}-differential yields of prompt J/ψ in the centrality classes 0–10% (left) and 30–50% (right), compared with different models, namely the statistical hadronisation model (SHMc) by Andronic et al. [36] and the Boltzmann transport model (BT) by Zhuang et al. [37, 85]. The bottom panels present the ratio of models to data, with the error bands representing the relative uncertainties originating from the models. For the computation of the ratio, an average value of the model is computed within the corresponding p_{T} intervals where the measurements are performed. Error bars around unity are the sum in quadrature of statistical and systematic uncertainties on the measured yields. In the SHMc model, the

JHEP02(2024)066

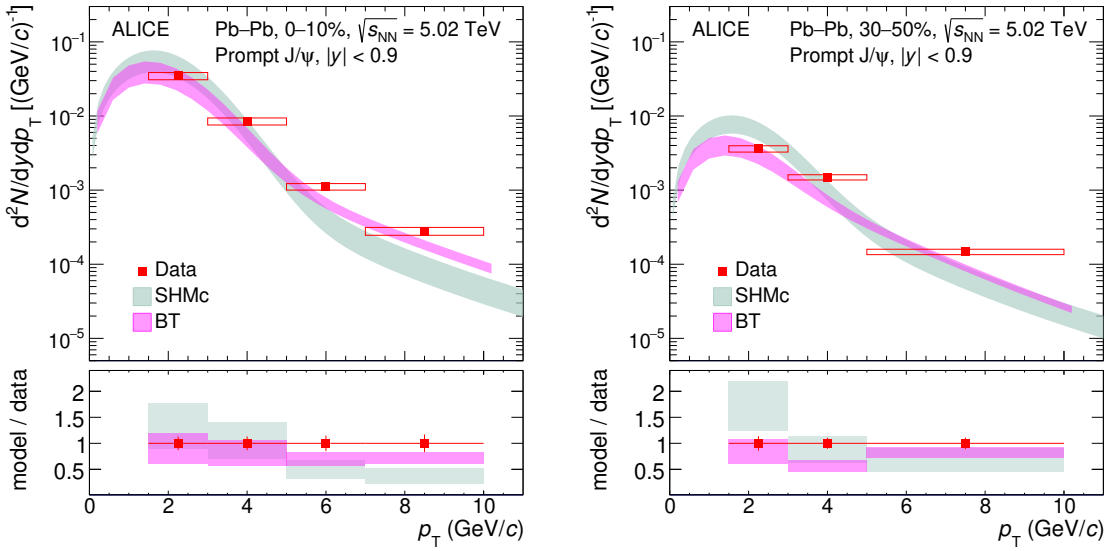

Figure 7. Prompt J/ψ yields as a function of p_{T} in the 0–10% (left panel) and 30–50% (right panel) centrality classes compared with models [36, 37, 85]. Vertical error bars and boxes represent statistical and systematic uncertainties, respectively. Shaded bands in the top panels represent model uncertainties. Bottom panels show the ratios between models and data, with the bands representing the relative uncertainties of the models. Error bars around unity are the quadratic sum of statistical and systematic uncertainties on the measured yields.

totality of charm quarks are produced in the initial hard parton–parton scatterings and thermalise inside the QGP. The total charm cross section employed in the SHMc calculations is the one measured by the ALICE collaboration in Pb–Pb collisions at $\sqrt{s_{\mathrm{NN}}} = 5.02\,\mathrm{TeV}$, extracted from open-charm meson production measurements [84]. Effects from CNM are taken into account when calculating the total number of charm quarks in Pb–Pb using rapidity dependent measurements of the nuclear modification factor of D mesons in proton–nucleus collisions [86], where interpolations, if necessary, are done via model calculations. The yield of the different bound states is determined by thermal weights computed at a common chemical freeze-out. The relative abundances of open and hidden charm hadrons are determined using the equilibrium thermodynamical parameters obtained from fits to the measured yields of light-flavoured hadrons and D-mesons, with the latter being used to extract the charm fugacity. The spectra in the SHMc model are obtained by coupling the hadron yields with a modified blast-wave function with input from hydrodynamical calculations for the flow profiles [36]. In the BT model, the total charm cross section in Pb–Pb collisions is evaluated from the charm-production cross section measured in pp collisions [87] scaled by the number of binary collisions, while to estimate CNM effects the EPS09 [88] gluon distributions are used. The dynamical evolution of the prompt charmonium states in the hot medium is described with a Boltzmann-type transport equation, including terms of dissociation and regeneration. The dissociation of charmonia inside the medium arises from the melting of the bound states due to colour Debye screening, as well as from collisional processes of charmonia with the medium constituents, and in particular from gluon dissociation. The regeneration cross section is connected to the dissociation cross section via the detailed balance between the

JHEP02(2024)066

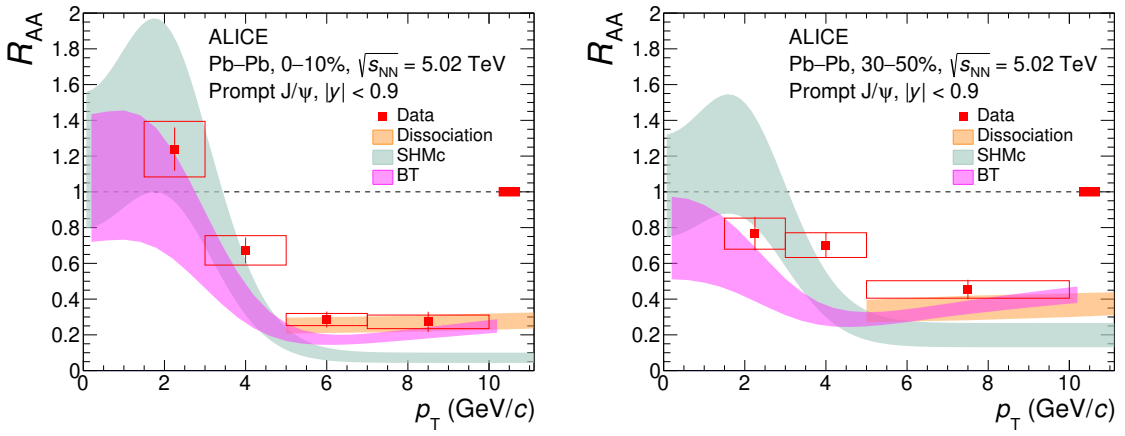

Figure 8. Prompt J/ψ $R_{\rm AA}$ as a function of $p_{\rm T}$ in the 0–10% (left panel) and 30–50% (right panel) centrality classes compared with models [36, 37, 85, 89, 90]. Error bars and boxes represent statistical and uncorrelated systematic uncertainties, respectively. Shaded bands represent model uncertainties. The global uncertainty is shown around unity.

gluon dissociation and reversed process. The model employs the (2+1)-dimensional version of the ideal hydrodynamic equations, including both a deconfined and a hadronic phase with a first order phase transition between these two. The uncertainties plotted in figure 7 for all models include contributions from total c$\bar{\rm c}$ cross section, as well as uncertainties from CNM assumptions. Both SHMc and BT models show an overall good agreement with data within uncertainties, in particular for $p_{\rm T}$ below 5 GeV/c. At higher $p_{\rm T}$, both models tend to underpredict the data, with the SHMc model showing a larger discrepancy, which is mainly due to the fact that in the SHMc model most of the produced J/ψ yields are thermal, with only a small contribution from the collision corona.

Figure 8 presents the prompt J/ψ nuclear modification factor as a function of $p_{\rm T}$ in the centrality class 0–10% (left panel) and 30–50% (right panel) compared with model calculations. In addition to the SHMc and BT models, prompt J/ψ $R_{\rm AA}$ measurements are also compared with the dissociation model by Vitev et al. [89]. In this model, which employs rate equations, the collisional dissociation of charmonia includes thermal effects on the wave function due to the screening of the c$\bar{\rm c}$ attractive potential from the free colour charges in the QGP. The medium is modelled by a (2+1)-dimensional viscous hydrodynamic model. Non-relativistic quantum chromodynamics (NRQCD) theory [91] is used to obtain the baseline nucleon–nucleon cross sections for charmonia and the $p_{\rm T}$-dependent feed-down from excited states. As this model provides predictions for $p_{\rm T} > 5$ GeV/c, the contribution from CNM effects is assumed to be negligible. The SHMc model reproduces the prompt J/ψ $R_{\rm AA}$ results at low $p_{\rm T}$ in both centrality classes, while it is significantly below the data for $p_{\rm T} > 5$ GeV/c. The BT model provides a good description of the measurements in the full $p_{\rm T}$ range in 0–10% most central collisions, while the model underpredicts the data in the centrality class 30–50%. The dissociation model, available only above 5 GeV/c, provides a good description of prompt J/ψ $R_{\rm AA}$ measurements within uncertainties.

JHEP02(2024)066

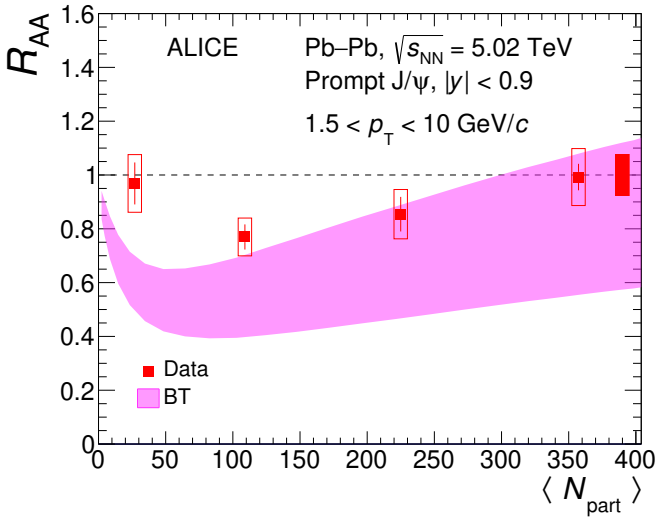

Figure 9. Centrality dependence (expressed in terms of average number of participants) of prompt J/ψ $R_{\rm AA}$ measured by ALICE in Pb–Pb collisions at $\sqrt{s_{\rm NN}} = 5.02$ TeV in the transverse momentum interval $1.5 < p_{\rm T} < 10\,{\rm GeV}/c$. Results are compared with the BT model by Zhuang et al. [37, 85]. Error bars and boxes represent statistical and uncorrelated systematic uncertainties, respectively. Shaded bands represent model uncertainties. The global uncertainty is shown around unity.

The centrality dependence of the $p_{\rm T}$-integrated ($1.5 < p_{\rm T} < 10\,{\rm GeV}/c$) $R_{\rm AA}$ of prompt J/ψ is compared with calculations from BT model in figure 9. The BT model, which shows a rising trend with increasing number of participants from $\langle N_{\rm part}\rangle \sim 50$, is in good agreement with experimental results in 0–10% and 10–30% centrality classes. Below $\langle N_{\rm part}\rangle \sim 50$, both the data and the model exhibit a similar increasing trend towards more peripheral collisions, however the agreement between data and model worsens.

4.4 Comparison with models for non-prompt J/ψ production

In the following, the comparison of non-prompt J/ψ measurements with models describing open heavy-flavour production is discussed. As both the production mechanisms and the interaction with the medium are significantly different for prompt charmonia and open heavy-flavour hadrons, non-prompt J/ψ measurements are compared with a different set of models with respect to those considered for prompt J/ψ results.

In figure 10, the yields of non-prompt J/ψ measured in the centralities 0–10% (left panel) and 30–50% (right panel), are compared with partonic transport model calculations [92–97]. The ratios of the models to data are depicted in the bottom panels, where the error bands are the model uncertainties. For computing the ratio, an average value of the model is considered within the corresponding $p_{\rm T}$ intervals where the measurements are performed. Error bars around unity are the quadratic sum of statistical and systematic uncertainties on the measured yields. In the transport model by Chen et al. [92] (LT1), as well as in the POWLANG transport model by Monteno et al. [93, 94], the Langevin equation is used for describing the evolution of the ancestor beauty quarks through the QGP. In POWLANG, transport coefficients are obtained either through perturbative calculations using the hard thermal loop (HTL)

JHEP02(2024)066

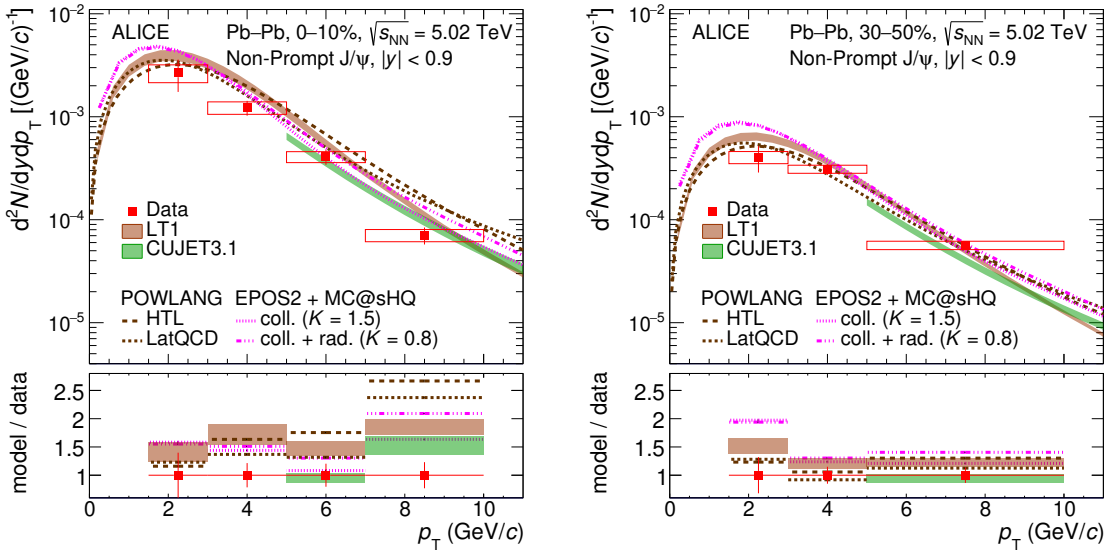

Figure 10. Non-prompt J/ψ yields as a function of p_{T} in the 0–10% (left panel) and 30–50% (right panel) centrality classes compared with models [92–97]. Vertical error bars and boxes represent statistical and systematic uncertainties, respectively. Shaded bands in the top panels represent model uncertainties where applicable. Bottom panels show the ratios between models and data, with the bands representing the relative uncertainties from the models. Error bars around unity are the quadratic sum of statistical and systematic uncertainties on the measured yields.

approach or calculations based on lattice QCD (LatQCD) simulations. The medium expansion is described by ideal (2+1)-dimensional hydrodynamic equations in LT1. In POWLANG, the background medium description is done via a (3+1)-dimensional hydrodynamic model, assuming no invariance for longitudinal boosts as considered in the (2+1)-dimensional case. The initial distribution of bottom quarks is parametrised according to perturbative-QCD calculations at fixed order with next-to-leading-log resummation (FONLL) [98] in LT1 and with the POWHEG-BOX package [99] in POWLANG. In both models, CNM effects are accounted for by using the EPS09 [88] gluon parton distribution functions, and at the hadronisation hypersurface, bottom and light-flavour quarks hadronise into beauty mesons via the coalescence model. In LT1, medium-induced gluon radiation is also included in the energy loss of heavy quarks, and becomes the dominant mechanism at large momentum, while in POWLANG the interactions of the heavy quarks with the medium constituents happen solely via collisional processes. In the calculations by Shi et al. [95, 96], the CUJET3.1 framework is used to evaluate the jet energy loss in a (2+1)-dimensional hydrodynamic background, implementing the contributions from collisional as well as from radiative processes. A set of R_{AA} and elliptic flow results from light hadrons in central and semicentral heavy-ion collisions is used to constrain the model, which is then used to predict heavy-flavour observables. For the initial p_{T} distribution of beauty quarks, FONLL calculations [98] with CTEQ6M [100] parton distribution functions are used. The formation of beauty hadrons happens via the classical vacuum-like fragmentation using the Peterson parametrisation in ref. [101]. In the model by Gossiaux et al. [97] (EPOS2+MC@sHQ), the Monte Carlo treatment of the Boltzmann equation of heavy quarks (MC@sHQ) [102] is coupled to a (3+1)-dimensional

JHEP02(2024)066

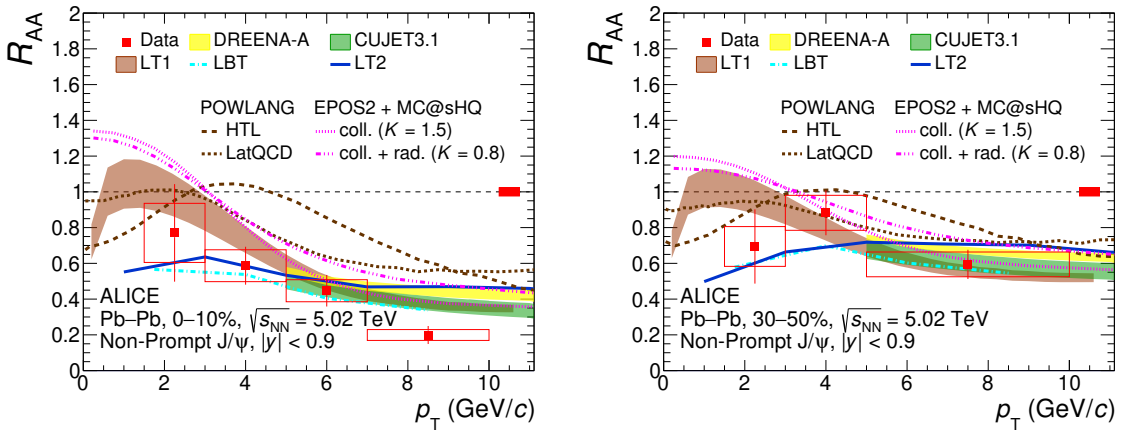

Figure 11. Non-prompt J/ψ $R_{\rm AA}$ as a function of $p_{\rm T}$ in the 0–10% (left panel) and 30–50% (right panel) centrality classes compared with models [92, 95–97, 105–108]. Error bars and boxes represent statistical and uncorrelated systematic uncertainties, respectively. Shaded bands represent model uncertainties where applicable. The global uncertainty is shown around unity.

fluid dynamical evolution of the locally thermalized QGP following the initial conditions from EPOS2 [103, 104]. The initial transverse momentum spectra of beauty quarks is obtained from FONLL calculations [98], and nuclear shadowing has been included according to the EPS09 [88] parametrization of the nuclear parton distribution functions. The calculations shown in this article consider two different configurations, either including pure collisional processes or both collisional and radiative ones. In order to further constrain the model, the corresponding cross sections are rescaled by a global factor K, which is chosen such that the predictions give a reasonable agreement at intermediate and high $p_{\rm T}$ with a set of D-meson $R_{\rm AA}$ measurements available in Pb–Pb collisions at $\sqrt{s_{\rm NN}} = 2.76$ TeV [97]. In particular, $K = 0.8$ (1.5) is considered when both collisional and radiative (pure collisional) processes are included. After the evolution in the medium, the beauty quarks hadronize via both fragmentation and coalescence. The LT1, POWLANG and EPOS2+MC@sHQ models show systematically higher values compared to data, for both centrality classes in the full measured transverse momentum range. The discrepancy looks larger for POWLANG, especially in centrality class 0–10% and at higher $p_{\rm T}$, which could be related to the absence of radiative processes in this model. The CUJET3.1 model, available only for $p_{\rm T}$ above 5 GeV/c, is compatible with the data within uncertainties.

The nuclear modification factor of non-prompt J/ψ is compared with models in figure 11 in 0–10% (left panel) and 30–50% (right panel) centrality intervals. The results are compared with the LT1, CUJET3.1, POWLANG and EPOS2+MC@sHQ models previously described as well as with additional ones [105–108]. In these additional calculations, the space–time evolution of the QGP is simulated using a (3+1)-dimensional viscous hydrodynamic model and both collisional and radiative energy loss mechanisms inside a thermal medium are considered. In the calculation by Li et al. [105], marked as LT2, the interactions between heavy quarks and the QGP are described by an improved Langevin approach. The transport model by Xing et al. [106] employs an extended linear Boltzmann transport (LBT) equation, which

JHEP02(2024)066

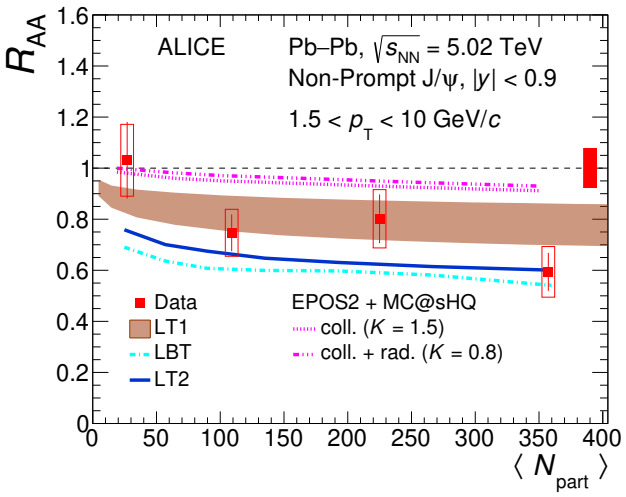

Figure 12. Centrality dependence (expressed in terms of average number of participants) of non-prompt J/ψ $R_{\rm AA}$ measured by ALICE in Pb–Pb collisions at $\sqrt{s_{\rm NN}} = 5.02\,\text{TeV}$ in the transverse momentum interval $1.5 < p_{\rm T} < 10\,\text{GeV}/c$. Results are compared with several partonic transport models [92, 97, 105, 106]. Error bars and boxes represent statistical and uncorrelated systematic uncertainties, respectively. Shaded bands represent model uncertainties where applicable. The global uncertainty is shown around unity.

includes both short and long-range interactions of heavy quarks with the QGP. In both LT2 and LBT models, the initial heavy quark $p_{\rm T}$ distribution is simulated according to FONLL calculations using CT14NLO [109] parton distribution functions modified according to the EPPS16 [110] next-to-leading-order parametrisation, while beauty hadrons are produced through a hybrid fragmentation–coalescence model [111]. The calculation by Djordjevic et al. [107, 108] employs a framework (DREENA-A) which combines the state-of-the-art dynamical energy loss model with hydrodynamical simulations. The initial heavy-quark spectrum is computed using next-to-leading-order calculations described in ref. [112] and KLP [113] fragmentation functions are used for the formation of beauty mesons. In both centralities all available model predictions except POWLANG show compatible values for $p_{\rm T}$ above $5\,\text{GeV}/c$, and within uncertainties are in an overall good agreement with the data. The POWLANG model overpredicts the $R_{\rm AA}$ in the centrality class 0–10% and at high $p_{\rm T}$, which might be a consequence of the lack of radiative energy loss contributions in this model. Below $5\,\text{GeV}/c$, the LT1 and POWLANG models sit on the upper side of the data points in both centrality classes, still being compatible with them within uncertainties, while the EPOS2+MC@sHQ model overpredicts the measurements. Both LBT and LT2 models are compatible with the measured $R_{\rm AA}$ within uncertainties in the full measured $p_{\rm T}$ range, and in both centrality classes.

Figure 12 depicts the non-prompt J/ψ $R_{\rm AA}$, integrated over $p_{\rm T}$ in the interval $1.5 < p_{\rm T} < 10\,\text{GeV}/c$, as a function of the number of participants in comparison with transport models. The LT1 model shows a slightly decreasing trend moving towards central collisions, and is compatible with data within uncertainties for all centrality classes. The LBT, LT2 and EPOS2+MC@sHQ models predict a similar decreasing trend for the non-prompt J/ψ $R_{\rm AA}$

JHEP02(2024)066

towards larger $\langle N_{\rm part} \rangle$. The LBT and LT2 models show good agreement with $R_{\rm AA}$ results in 0–10% centrality class, while for other centrality classes both models slightly underpredict the data. The EPOS2+MC@sHQ model agrees with measured $R_{\rm AA}$ in the most peripheral class, while it tends to overestimate measurements towards more central collisions.

5 Summary

Prompt and non-prompt J/ψ production is measured by the ALICE collaboration in Pb–Pb collisions at $\sqrt{s_{\rm NN}} = 5.02\,\text{TeV}$ in the rapidity interval $|y| < 0.9$ as a function of $p_{\rm T}$ and centrality. In particular, $p_{\rm T}$-differential measurements of non-prompt J/ψ fractions, production yields, and nuclear modification factors are carried out. The ALICE results extend the existing CMS and ATLAS measurements at midrapidity, available only at high $p_{\rm T}$, down to $p_{\rm T} = 1.5\,\text{GeV}/c$, and all measurements look compatible within uncertainties in the common $p_{\rm T}$ intervals. Non-prompt J/ψ fractions show a rising trend with increasing $p_{\rm T}$, similar to the one observed in pp collisions, while no significant dependence on the centrality is observed within uncertainties, with the exception of most central collisions where $f_{\rm B}$ exhibits a significant decrease with respect to other centrality classes. The comparison with earlier measurements in Pb–Pb collisions at $\sqrt{s_{\rm NN}} = 2.76\,\text{TeV}$ shows compatible results at the two centre-of-mass energies and highlights a significantly improved precision with Run 2 data.

For $p_{\rm T} > 5\,\text{GeV}/c$, the prompt J/$\psi$ $R_{\rm AA}$ decreases with increasing centrality, while at lower $p_{\rm T}$ the suppression is smaller in 0–10% most central collisions, in particular in the lowest $p_{\rm T}$ interval where the prompt J/ψ $R_{\rm AA}$ exceeds unity. These results are consistent with $p_{\rm T}$-integrated measurements of prompt J/ψ $R_{\rm AA}$, which rises with $\langle N_{\rm part} \rangle$, hinting at an increasing contribution from regeneration at low $p_{\rm T}$ and more central collisions. In 0–10% most central collisions, the SHMc model and transport microscopic calculations that include a contribution from regeneration are compatible with experimental data for $p_{\rm T} < 5\,\text{GeV}/c$. However, at higher $p_{\rm T}$, transport models are compatible with the measurements within uncertainties, while the SHMc model significantly underpredicts the data. In semicentral collisions there is less agreement between data and models. In particular, for $p_{\rm T}$ above $3\,\text{GeV}/c$ the models either underpredict the data or sit at the lower edge of the experimental uncertainty.

The non-prompt J/ψ $R_{\rm AA}$ integrated over $p_{\rm T}$ hints at a decreasing trend towards more central collisions. As a function of $p_{\rm T}$, the non-prompt J/ψ $R_{\rm AA}$ in different centrality classes are compatible within uncertainties below $5\,\text{GeV}/c$, while at higher $p_{\rm T}$ the suppression is larger in the centrality interval 0–10%. Results are consistent within uncertainties with non-prompt $\rm D^0$ $R_{\rm AA}$ measurements in the centrality classes 0–10% and 30–50%. Several transport models are able to describe the data within uncertainties. All calculations, but POWLANG, implement both collisional and radiative energy loss processes combined with a dynamically expanding QGP, considering different hypotheses on transport dynamics, CNM effects, $p_{\rm T}$ distributions and hadronisation of beauty quarks. Above $5\,\text{GeV}/c$, all calculations predict a similar suppression for non-prompt J/ψ and are consistent with the data within uncertainties, with the exception of POWLANG, which overpredicts the data in most central events. This points to the importance of radiative energy loss contributions in the high-$p_{\rm T}$ region. At lower $p_{\rm T}$ and for the $p_{\rm T}$-integrated case, theoretical calculations predict different magnitudes of the suppression. However, due to the current precision of the measurements it is not possible to discriminate among them as all calculations are compatible with the data within uncertainties.

JHEP02(2024)066

Both prompt and non-prompt J/ψ measurements will improve significantly taking advantage of the larger expected data sample and the better spatial resolution provided at midrapidity by the upgraded ITS [114] in the next LHC runs. In particular, further differential measurements in the non-prompt charmonium sector, in addition to yet unmeasured observables such as the elliptic flow, could allow further constraining different open beauty hadron production models.

Acknowledgments

The ALICE Collaboration would like to thank all its engineers and technicians for their invaluable contributions to the construction of the experiment and the CERN accelerator teams for the outstanding performance of the LHC complex. The ALICE Collaboration gratefully acknowledges the resources and support provided by all Grid centres and the Worldwide LHC Computing Grid (WLCG) collaboration. The ALICE Collaboration acknowledges the following funding agencies for their support in building and running the ALICE detector: A. I. Alikhanyan National Science Laboratory (Yerevan Physics Institute) Foundation (ANSL), State Committee of Science and World Federation of Scientists (WFS), Armenia; Austrian Academy of Sciences, Austrian Science Fund (FWF): [M 2467-N36] and Nationalstiftung für Forschung, Technologie und Entwicklung, Austria; Ministry of Communications and High Technologies, National Nuclear Research Center, Azerbaijan; Conselho Nacional de Desenvolvimento Científico e Tecnológico (CNPq), Financiadora de Estudos e Projetos (Finep), Fundação de Amparo à Pesquisa do Estado de São Paulo (FAPESP) and Universidade Federal do Rio Grande do Sul (UFRGS), Brazil; Bulgarian Ministry of Education and Science, within the National Roadmap for Research Infrastructures 2020-2027 (object CERN), Bulgaria; Ministry of Education of China (MOEC) , Ministry of Science & Technology of China (MSTC) and National Natural Science Foundation of China (NSFC), China; Ministry of Science and Education and Croatian Science Foundation, Croatia; Centro de Aplicaciones Tecnológicas y Desarrollo Nuclear (CEADEN), Cubaenergía, Cuba; Ministry of Education, Youth and Sports of the Czech Republic, Czech Republic; The Danish Council for Independent Research | Natural Sciences, the VILLUM FONDEN and Danish National Research Foundation (DNRF), Denmark; Helsinki Institute of Physics (HIP), Finland; Commissariat à l'Energie Atomique (CEA) and Institut National de Physique Nucléaire et de Physique des Particules (IN2P3) and Centre National de la Recherche Scientifique (CNRS), France; Bundesministerium für Bildung und Forschung (BMBF) and GSI Helmholtzzentrum für Schwerionenforschung GmbH, Germany; General Secretariat for Research and Technology, Ministry of Education, Research and Religions, Greece; National Research, Development and Innovation Office, Hungary; Department of Atomic Energy Government of India (DAE), Department of Science and Technology, Government of India (DST), University Grants Commission, Government of India (UGC) and Council of Scientific and Industrial Research (CSIR), India; National Research and Innovation Agency - BRIN, Indonesia; Istituto Nazionale di Fisica Nucleare (INFN), Italy; Japanese Ministry of Education, Culture, Sports, Science and Technology (MEXT) and Japan Society for the Promotion of Science (JSPS) KAKENHI, Japan; Consejo Nacional de Ciencia (CONACYT) y Tecnología, through Fondo de Cooperación Internacional en Ciencia y Tecnología (FONCICYT) and Dirección General de Asuntos del Personal

JHEP02(2024)066

Academico (DGAPA), Mexico; Nederlandse Organisatie voor Wetenschappelijk Onderzoek (NWO), Netherlands; The Research Council of Norway, Norway; Commission on Science and Technology for Sustainable Development in the South (COMSATS), Pakistan; Pontificia Universidad Católica del Perú, Peru; Ministry of Education and Science, National Science Centre and WUT ID-UB, Poland; Korea Institute of Science and Technology Information and National Research Foundation of Korea (NRF), Republic of Korea; Ministry of Education and Scientific Research, Institute of Atomic Physics, Ministry of Research and Innovation and Institute of Atomic Physics and University Politehnica of Bucharest, Romania; Ministry of Education, Science, Research and Sport of the Slovak Republic, Slovakia; National Research Foundation of South Africa, South Africa; Swedish Research Council (VR) and Knut & Alice Wallenberg Foundation (KAW), Sweden; European Organization for Nuclear Research, Switzerland; Suranaree University of Technology (SUT), National Science and Technology Development Agency (NSTDA), Thailand Science Research and Innovation (TSRI) and National Science, Research and Innovation Fund (NSRF), Thailand; Turkish Energy, Nuclear and Mineral Research Agency (TENMAK), Turkey; National Academy of Sciences of Ukraine, Ukraine; Science and Technology Facilities Council (STFC), United Kingdom; National Science Foundation of the United States of America (NSF) and United States Department of Energy, Office of Nuclear Physics (DOE NP), United States of America. In addition, individual groups or members have received support from: European Research Council, Strong 2020 — Horizon 2020 (grant nos. 950692, 824093), European Union; Academy of Finland (Center of Excellence in Quark Matter) (grant nos. 346327, 346328), Finland.

JHEP02(2024)066

References

[1] F. Karsch, *Lattice simulations of the thermodynamics of strongly interacting elementary particles and the exploration of new phases of matter in relativistic heavy ion collisions*, *J. Phys. Conf. Ser.* **46** (2006) 122 [hep-lat/0608003] [INSPIRE].

[2] WUPPERTAL-BUDAPEST collaboration, *Is there still any T_c mystery in lattice QCD? Results with physical masses in the continuum limit III*, *JHEP* **09** (2010) 073 [arXiv:1005.3508] [INSPIRE].

[3] S. Borsanyi et al., *Full result for the QCD equation of state with $2+1$ flavors*, *Phys. Lett. B* **730** (2014) 99 [arXiv:1309.5258] [INSPIRE].

[4] A. Bazavov et al., *The chiral and deconfinement aspects of the QCD transition*, *Phys. Rev. D* **85** (2012) 054503 [arXiv:1111.1710] [INSPIRE].

[5] T. Csorgo, *New form of matter at CERN SPS: Quark matter but not quark gluon plasma*, *Nucl. Phys. B Proc. Suppl.* **92** (2001) 62 [hep-ph/0011339] [INSPIRE].

[6] D. Teaney, J. Lauret and E.V. Shuryak, *Flow at the SPS and RHIC as a quark gluon plasma signature*, *Phys. Rev. Lett.* **86** (2001) 4783 [nucl-th/0011058] [INSPIRE].

[7] BRAHMS collaboration, *Quark gluon plasma and color glass condensate at RHIC? The Perspective from the BRAHMS experiment*, *Nucl. Phys. A* **757** (2005) 1 [nucl-ex/0410020] [INSPIRE].

[8] PHOBOS collaboration, *The PHOBOS perspective on discoveries at RHIC*, *Nucl. Phys. A* **757** (2005) 28 [nucl-ex/0410022] [INSPIRE].

[9] STAR collaboration, *Experimental and theoretical challenges in the search for the quark gluon plasma: The STAR Collaboration's critical assessment of the evidence from RHIC collisions*, *Nucl. Phys. A* **757** (2005) 102 [nucl-ex/0501009] [INSPIRE].

[10] PHENIX collaboration, *Formation of dense partonic matter in relativistic nucleus-nucleus collisions at RHIC: Experimental evaluation by the PHENIX collaboration*, *Nucl. Phys. A* **757** (2005) 184 [nucl-ex/0410003] [INSPIRE].

[11] ALICE collaboration, *The ALICE experiment — A journey through QCD*, arXiv:2211.04384 [INSPIRE].

[12] A. Andronic et al., *Heavy-flavour and quarkonium production in the LHC era: from proton-proton to heavy-ion collisions*, *Eur. Phys. J. C* **76** (2016) 107 [arXiv:1506.03981] [INSPIRE].

[13] F.-M. Liu and S.-X. Liu, *Quark-gluon plasma formation time and direct photons from heavy ion collisions*, *Phys. Rev. C* **89** (2014) 034906 [arXiv:1212.6587] [INSPIRE].

[14] T. Matsui and H. Satz, *J/ψ Suppression by Quark-Gluon Plasma Formation*, *Phys. Lett. B* **178** (1986) 416 [INSPIRE].

[15] A. Rothkopf, *Heavy Quarkonium in Extreme Conditions*, *Phys. Rept.* **858** (2020) 1 [arXiv:1912.02253] [INSPIRE].

[16] NA38 collaboration, *ψ' and J/ψ production in p-W, p-U and S-U interactions at 200-GeV/nucleon*, *Phys. Lett. B* **345** (1995) 617 [INSPIRE].

[17] NA50 collaboration, *A New measurement of J/ψ suppression in Pb-Pb collisions at 158-GeV per nucleon*, *Eur. Phys. J. C* **39** (2005) 335 [hep-ex/0412036] [INSPIRE].

[18] PHENIX collaboration, *J/ψ Production vs Centrality, Transverse Momentum, and Rapidity in Au+Au Collisions at $\sqrt{s_{NN}} = 200$ GeV*, *Phys. Rev. Lett.* **98** (2007) 232301 [nucl-ex/0611020] [INSPIRE].

[19] PHENIX collaboration, *J/ψ suppression at forward rapidity in Au+Au collisions at $\sqrt{s_{NN}} = 200$ GeV*, *Phys. Rev. C* **84** (2011) 054912 [arXiv:1103.6269] [INSPIRE].

[20] STAR collaboration, *J/ψ production at high transverse momentum in p+p and Cu+Cu collisions at $\sqrt{s_{\rm NN}} = 200$ GeV*, *Phys. Rev. C* **80** (2009) 041902 [arXiv:0904.0439] [INSPIRE].

[21] STAR collaboration, *J/ψ production at low p_T in Au + Au and Cu + Cu collisions at $\sqrt{s_{NN}} = 200$ GeV with the STAR detector*, *Phys. Rev. C* **90** (2014) 024906 [arXiv:1310.3563] [INSPIRE].

[22] CMS collaboration, *Suppression of Non-Prompt J/ψ, Prompt J/ψ, and Y(1S) in PbPb Collisions at $\sqrt{s_{NN}} = 2.76$ TeV*, *JHEP* **05** (2012) 063 [arXiv:1201.5069] [INSPIRE].

[23] ALICE collaboration, *J/ψ suppression at forward rapidity in Pb-Pb collisions at $\sqrt{s_{NN}} = 2.76$ TeV*, *Phys. Rev. Lett.* **109** (2012) 072301 [arXiv:1202.1383] [INSPIRE].

[24] ALICE collaboration, *Centrality, rapidity and transverse momentum dependence of J/ψ suppression in Pb-Pb collisions at $\sqrt{s_{\rm NN}} = 2.76$ TeV*, *Phys. Lett. B* **734** (2014) 314 [arXiv:1311.0214] [INSPIRE].

JHEP02(2024)066

[25] ALICE collaboration, *Differential studies of inclusive J/ψ $\psi(2S)$ production at forward rapidity in Pb-Pb collisions at $\sqrt{s_{\rm NN}} = 2.76$ TeV*, *JHEP* **05** (2016) 179 [arXiv:1506.08804] [INSPIRE].

[26] ALICE collaboration, *J/ψ suppression at forward rapidity in Pb-Pb collisions at $\sqrt{s_{\rm NN}} = 5.02$ TeV*, *Phys. Lett. B* **766** (2017) 212 [arXiv:1606.08197] [INSPIRE].

[27] ALICE collaboration, *Studies of J/ψ production at forward rapidity in Pb-Pb collisions at $\sqrt{s_{\rm NN}} = 5.02$ TeV*, *JHEP* **02** (2020) 041 [arXiv:1909.03158] [INSPIRE].

[28] ALICE collaboration, *Centrality and transverse momentum dependence of inclusive J/ψ production at midrapidity in Pb-Pb collisions at $sNN = 5.02$ TeV*, *Phys. Lett. B* **805** (2020) 135434 [arXiv:1910.14404] [INSPIRE].

[29] ATLAS collaboration, *Prompt and non-prompt J/ψ and ψ(2S) suppression at high transverse momentum in* 5.02 TeV *Pb+Pb collisions with the ATLAS experiment*, *Eur. Phys. J. C* **78** (2018) 762 [arXiv:1805.04077] [INSPIRE].

[30] CMS collaboration, *Measurement of prompt and nonprompt charmonium suppression in PbPb collisions at 5.02TeV*, *Eur. Phys. J. C* **78** (2018) 509 [arXiv:1712.08959] [INSPIRE].

[31] ALICE collaboration, *Measurements of inclusive J/ψ production at midrapidity and forward rapidity in Pb-Pb collisions at $sNN = 5.02$ TeV*, *Phys. Lett. B* **849** (2024) 138451 [arXiv:2303.13361] [INSPIRE].

[32] P. Braun-Munzinger and J. Stachel, *(Non)thermal aspects of charmonium production and a new look at J/ψ suppression*, *Phys. Lett. B* **490** (2000) 196 [nucl-th/0007059] [INSPIRE].

[33] R.L. Thews, M. Schroedter and J. Rafelski, *Enhanced J/ψ production in deconfined quark matter*, *Phys. Rev. C* **63** (2001) 054905 [hep-ph/0007323] [INSPIRE].

[34] ALICE collaboration, *J/ψ elliptic and triangular flow in Pb-Pb collisions at $\sqrt{s_{\rm NN}} = 5.02$ TeV*, *JHEP* **10** (2020) 141 [arXiv:2005.14518] [INSPIRE].

[35] ALICE collaboration, *J/ψ elliptic flow in Pb-Pb collisions at $\sqrt{s_{\rm NN}} = 5.02$ TeV*, *Phys. Rev. Lett.* **119** (2017) 242301 [arXiv:1709.05260] [INSPIRE].

[36] A. Andronic et al., *Transverse momentum distributions of charmonium states with the statistical hadronization model*, *Phys. Lett. B* **797** (2019) 134836 [arXiv:1901.09200] [INSPIRE].

[37] K. Zhou, N. Xu, Z. Xu and P. Zhuang, *Medium effects on charmonium production at ultrarelativistic energies available at the CERN Large Hadron Collider*, *Phys. Rev. C* **89** (2014) 054911 [arXiv:1401.5845] [INSPIRE].

[38] X. Du and R. Rapp, *Sequential Regeneration of Charmonia in Heavy-Ion Collisions*, *Nucl. Phys. A* **943** (2015) 147 [arXiv:1504.00670] [INSPIRE].

[39] ALICE collaboration, *$\psi(2S)$ Suppression in Pb-Pb Collisions at the LHC*, *Phys. Rev. Lett.* **132** (2024) 042301 [arXiv:2210.08893] [INSPIRE].

[40] M. He, H. van Hees and R. Rapp, *Heavy-quark diffusion in the quark-gluon plasma*, *Prog. Part. Nucl. Phys.* **130** (2023) 104020 [arXiv:2204.09299] [INSPIRE].

[41] M. Gyulassy and M. Plumer, *Jet Quenching in Dense Matter*, *Phys. Lett. B* **243** (1990) 432 [INSPIRE].

[42] R. Baier et al., *Radiative energy loss and $p_{\rm T}$ broadening of high-energy partons in nuclei*, *Nucl. Phys. B* **484** (1997) 265 [hep-ph/9608322] [INSPIRE].

[43] M.H. Thoma and M. Gyulassy, *Quark Damping and Energy Loss in the High Temperature QCD*, *Nucl. Phys. B* **351** (1991) 491 [INSPIRE].

JHEP02(2024)066

[44] E. Braaten and M.H. Thoma, *Energy loss of a heavy fermion in a hot plasma*, *Phys. Rev. D* **44** (1991) 1298 [INSPIRE].

[45] E. Braaten and M.H. Thoma, *Energy loss of a heavy quark in the quark-gluon plasma*, *Phys. Rev. D* **44** (1991) R2625 [INSPIRE].

[46] Y.L. Dokshitzer and D.E. Kharzeev, *Heavy quark colorimetry of QCD matter*, *Phys. Lett. B* **519** (2001) 199 [hep-ph/0106202] [INSPIRE].

[47] N. Armesto, C.A. Salgado and U.A. Wiedemann, *Medium induced gluon radiation off massive quarks fills the dead cone*, *Phys. Rev. D* **69** (2004) 114003 [hep-ph/0312106] [INSPIRE].

[48] S. Wicks, W. Horowitz, M. Djordjevic and M. Gyulassy, *Heavy quark jet quenching with collisional plus radiative energy loss and path length fluctuations*, *Nucl. Phys. A* **783** (2007) 493 [nucl-th/0701063] [INSPIRE].

[49] R.J. Fries, B. Muller, C. Nonaka and S.A. Bass, *Hadronization in heavy ion collisions: Recombination and fragmentation of partons*, *Phys. Rev. Lett.* **90** (2003) 202303 [nucl-th/0301087] [INSPIRE].

[50] L. Ravagli and R. Rapp, *Quark Coalescence based on a Transport Equation*, *Phys. Lett. B* **655** (2007) 126 [arXiv:0705.0021] [INSPIRE].

[51] V. Greco, C.M. Ko and R. Rapp, *Quark coalescence for charmed mesons in ultrarelativistic heavy ion collisions*, *Phys. Lett. B* **595** (2004) 202 [nucl-th/0312100] [INSPIRE].

[52] N. Armesto, *Nuclear shadowing*, *J. Phys. G* **32** (2006) R367 [hep-ph/0604108] [INSPIRE].

[53] ALICE collaboration, *Inclusive, prompt and non-prompt J/ψ production at midrapidity in p-Pb collisions at $\sqrt{s_{\rm NN}} = 5.02$ TeV*, *JHEP* **06** (2022) 011 [arXiv:2105.04957] [INSPIRE].

[54] ALICE collaboration, *Inclusive, prompt and non-prompt J/ψ production at mid-rapidity in Pb-Pb collisions at $\sqrt{s_{\rm NN}} = 2.76$ TeV*, *JHEP* **07** (2015) 051 [arXiv:1504.07151] [INSPIRE].

[55] ALICE collaboration, *The ALICE experiment at the CERN LHC*, 2008 *JINST* **3** S08002 [INSPIRE].

[56] ALICE collaboration, *Performance of the ALICE Experiment at the CERN LHC*, *Int. J. Mod. Phys. A* **29** (2014) 1430044 [arXiv:1402.4476] [INSPIRE].

[57] J. Alme et al., *The ALICE TPC, a large 3-dimensional tracking device with fast readout for ultra-high multiplicity events*, *Nucl. Instrum. Meth. A* **622** (2010) 316 [arXiv:1001.1950] [INSPIRE].

[58] ALICE collaboration, *Performance of the ALICE VZERO system*, 2013 *JINST* **8** P10016 [arXiv:1306.3130] [INSPIRE].

[59] ALICE collaboration, *Performance of the ALICE Zero Degree Calorimeters and upgrade strategy*, *J. Phys. Conf. Ser.* **1162** (2019) 012006 [INSPIRE].

[60] ALICE collaboration, *Centrality determination in heavy ion collisions*, ALICE-PUBLIC-2018-011 (2018) [INSPIRE].

[61] R.J. Glauber and G. Matthiae, *High-energy scattering of protons by nuclei*, *Nucl. Phys. B* **21** (1970) 135 [INSPIRE].

[62] M.L. Miller, K. Reygers, S.J. Sanders and P. Steinberg, *Glauber modeling in high energy nuclear collisions*, *Ann. Rev. Nucl. Part. Sci.* **57** (2007) 205 [nucl-ex/0701025] [INSPIRE].

[63] D. d'Enterria and C. Loizides, *Progress in the Glauber Model at Collider Energies*, *Ann. Rev. Nucl. Part. Sci.* **71** (2021) 315 [arXiv:2011.14909] [INSPIRE].

JHEP02(2024)066

[64] C. Loizides, J. Kamin and D. d'Enterria, *Improved Monte Carlo Glauber predictions at present and future nuclear colliders*, *Phys. Rev. C* **97** (2018) 054910 [*Erratum ibid.* **99** (2019) 019901] [arXiv:1710.07098] [INSPIRE].

[65] ALICE collaboration, *J/ψ production at midrapidity in p−Pb collisions at $\sqrt{s_{\rm NN}} = 8.16$ TeV*, *JHEP* **07** (2023) 137 [arXiv:2211.14153] [INSPIRE].

[66] ALICE collaboration, *Prompt and non-prompt J/ψ production and nuclear modification at mid-rapidity in p-Pb collisions at $\sqrt{s_{NN}} = 5.02$ TeV*, *Eur. Phys. J. C* **78** (2018) 466 [arXiv:1802.00765] [INSPIRE].

[67] ALICE collaboration, *Prompt and non-prompt J/ψ production cross sections at midrapidity in proton-proton collisions at $\sqrt{\rm s} = 5.02$ and 13 TeV*, *JHEP* **03** (2022) 190 [arXiv:2108.02523] [INSPIRE].

[68] Particle Data Group collaboration, *Review of Particle Physics*, *PTEP* **2022** (2022) 083C01 [INSPIRE].

[69] X.-N. Wang and M. Gyulassy, *HIJING: A Monte Carlo model for multiple jet production in* pp*,* pA*, and* AA *collisions*, *Phys. Rev. D* **44** (1991) 3501 [INSPIRE].

[70] T. Sjostrand, S. Mrenna and P.Z. Skands, *PYTHIA 6.4 Physics and Manual*, *JHEP* **05** (2006) 026 [hep-ph/0603175] [INSPIRE].

[71] D.J. Lange, *The EvtGen particle decay simulation package*, *Nucl. Instrum. Meth. A* **462** (2001) 152 [INSPIRE].

[72] E. Barberio and Z. Was, *PHOTOS: A Universal Monte Carlo for QED radiative corrections. Version 2.0*, *Comput. Phys. Commun.* **79** (1994) 291 [INSPIRE].

[73] ALICE collaboration, *Measurement of the inclusive J/ψ polarization at forward rapidity in pp collisions at $\sqrt{\rm s} = 8$ TeV*, *Eur. Phys. J. C* **78** (2018) 562 [arXiv:1805.04374] [INSPIRE].

[74] ALICE collaboration, *First measurement of quarkonium polarization in nuclear collisions at the LHC*, *Phys. Lett. B* **815** (2021) 136146 [arXiv:2005.11128] [INSPIRE].

[75] R. Brun et al., *GEANT Detector Description and Simulation Tool*, CERN-W5013 (1994) [DOI:10.17181/CERN.MUHF.DMJ1] [INSPIRE].

[76] J.E. Gaiser, *Charmonium Spectroscopy From Radiative Decays of the J/ψ and ψ'*, Ph.D. thesis, SLAC, Stanford, U.S.A. (1982) [INSPIRE].

[77] CDF collaboration, *Measurement of the J/ψ meson and b−hadron production cross sections in $p\bar{p}$ collisions at $\sqrt{s} = 1960$ GeV*, *Phys. Rev. D* **71** (2005) 032001 [hep-ex/0412071] [INSPIRE].

[78] CMS collaboration, *Measurement of prompt and nonprompt* J/ψ *production in* pp *and* pPb *collisions at $\sqrt{s_{\rm NN}} = 5.02$ TeV*, *Eur. Phys. J. C* **77** (2017) 269 [arXiv:1702.01462] [INSPIRE].

[79] ALICE collaboration, *Measurement of prompt J/ψ and beauty hadron production cross sections at mid-rapidity in pp collisions at $\sqrt{s} = 7$ TeV*, *JHEP* **11** (2012) 065 [arXiv:1205.5880] [INSPIRE].

[80] ATLAS collaboration, *Measurement of the differential cross-sections of prompt and non-prompt production of J/ψ and ψ(2S) in pp collisions at $\sqrt{s} = 7$ and 8 TeV with the ATLAS detector*, *Eur. Phys. J. C* **76** (2016) 283 [arXiv:1512.03657] [INSPIRE].

[81] ATLAS collaboration, *Measurement of the differential cross-sections of inclusive, prompt and non-prompt J/ψ production in proton-proton collisions at $\sqrt{s} = 7$ TeV*, *Nucl. Phys. B* **850** (2011) 387 [arXiv:1104.3038] [INSPIRE].

JHEP02(2024)066

[82] CMS collaboration, *Prompt and Non-Prompt J/ψ Production in pp Collisions at $\sqrt{s} = 7$ TeV*, *Eur. Phys. J. C* **71** (2011) 1575 [arXiv:1011.4193] [INSPIRE].

[83] ALICE collaboration, *Inclusive J/ψ production at mid-rapidity in pp collisions at $\sqrt{s} = 5.02$ TeV*, *JHEP* **10** (2019) 084 [arXiv:1905.07211] [INSPIRE].

[84] ALICE collaboration, *Measurement of beauty production via non-prompt D^0 mesons in Pb-Pb collisions at $\sqrt{s_{NN}} = 5.02$ TeV*, *JHEP* **12** (2022) 126 [arXiv:2202.00815] [INSPIRE].

[85] B. Chen, *Thermal production of charmonia in Pb-Pb collisions at $\sqrt{s_{NN}} = 5.02$ TeV*, *Chin. Phys. C* **43** (2019) 124101 [arXiv:1811.11393] [INSPIRE].

[86] LHCb collaboration, *Study of prompt D^0 meson production in pPb collisions at $\sqrt{s_{\rm NN}} = 5$ TeV*, *JHEP* **10** (2017) 090 [arXiv:1707.02750] [INSPIRE].

[87] ALICE collaboration, *Charm-quark fragmentation fractions and production cross section at midrapidity in pp collisions at the LHC*, *Phys. Rev. D* **105** (2022) L011103 [arXiv:2105.06335] [INSPIRE].

[88] K.J. Eskola, H. Paukkunen and C.A. Salgado, *EPS09: A New Generation of NLO and LO Nuclear Parton Distribution Functions*, *JHEP* **04** (2009) 065 [arXiv:0902.4154] [INSPIRE].

[89] S. Aronson et al., *Collisional and thermal dissociation of J/ψ and Υ states at the LHC*, *Phys. Lett. B* **778** (2018) 384 [arXiv:1709.02372] [INSPIRE].

[90] Y. Makris and I. Vitev, *An Effective Theory of Quarkonia in QCD Matter*, *JHEP* **10** (2019) 111 [arXiv:1906.04186] [INSPIRE].

[91] G.T. Bodwin, E. Braaten and G.P. Lepage, *Rigorous QCD analysis of inclusive annihilation and production of heavy quarkonium*, *Phys. Rev. D* **51** (1995) 1125 [*Erratum ibid.* **55** (1997) 5853] [hep-ph/9407339] [INSPIRE].

[92] M. Yang et al., *Bottom energy loss and nonprompt J/ψ production in relativistic heavy ion collisions*, *Phys. Rev. C* **107** (2023) 054917 [arXiv:2302.06179] [INSPIRE].

[93] A. Beraudo et al., *Rapidity dependence of heavy-flavour production in heavy-ion collisions within a full $3+1$ transport approach: quenching, elliptic and directed flow*, *JHEP* **05** (2021) 279 [arXiv:2102.08064] [INSPIRE].

[94] A. Beraudo et al., *Heavy flavors in heavy-ion collisions: quenching, flow and correlations*, *Eur. Phys. J. C* **75** (2015) 121 [arXiv:1410.6082] [INSPIRE].

[95] S. Shi, J. Liao and M. Gyulassy, *Global constraints from RHIC and LHC on transport properties of QCD fluids in CUJET/CIBJET framework*, *Chin. Phys. C* **43** (2019) 044101 [arXiv:1808.05461] [INSPIRE].

[96] S. Shi, J. Liao and M. Gyulassy, *Probing the Color Structure of the Perfect QCD Fluids via Soft-Hard-Event-by-Event Azimuthal Correlations*, *Chin. Phys. C* **42** (2018) 104104 [arXiv:1804.01915] [INSPIRE].

[97] M. Nahrgang, J. Aichelin, P.B. Gossiaux and K. Werner, *Toward a consistent evolution of the quark-gluon plasma and heavy quarks*, *Phys. Rev. C* **93** (2016) 044909 [arXiv:1602.03544] [INSPIRE].

[98] M. Cacciari, P. Nason and R. Vogt, *QCD predictions for charm and bottom production at RHIC*, *Phys. Rev. Lett.* **95** (2005) 122001 [hep-ph/0502203] [INSPIRE].

[99] S. Frixione, P. Nason and G. Ridolfi, *A Positive-weight next-to-leading-order Monte Carlo for heavy flavour hadroproduction*, *JHEP* **09** (2007) 126 [arXiv:0707.3088] [INSPIRE].

JHEP02(2024)066

[100] J. Pumplin et al., *New generation of parton distributions with uncertainties from global QCD analysis*, *JHEP* **07** (2002) 012 [hep-ph/0201195] [INSPIRE].

[101] C. Peterson, D. Schlatter, I. Schmitt and P.M. Zerwas, *Scaling Violations in Inclusive e^+e^- Annihilation Spectra*, *Phys. Rev. D* **27** (1983) 105 [INSPIRE].

[102] P.B. Gossiaux and J. Aichelin, *Towards an understanding of the RHIC single electron data*, *Phys. Rev. C* **78** (2008) 014904 [arXiv:0802.2525] [INSPIRE].

[103] K. Werner et al., *Event-by-Event Simulation of the Three-Dimensional Hydrodynamic Evolution from Flux Tube Initial Conditions in Ultrarelativistic Heavy Ion Collisions*, *Phys. Rev. C* **82** (2010) 044904 [arXiv:1004.0805] [INSPIRE].

[104] K. Werner et al., *Jets, Bulk Matter, and their Interaction in Heavy Ion Collisions at Several TeV*, *Phys. Rev. C* **85** (2012) 064907 [arXiv:1203.5704] [INSPIRE].

[105] S.-Q. Li et al., *Scaling behaviors of heavy flavor meson suppression and flow in different nuclear collision systems at the LHC*, *Eur. Phys. J. C* **81** (2021) 1035 [arXiv:2108.06648] [INSPIRE].

[106] W.-J. Xing, G.-Y. Qin and S. Cao, *Perturbative and non-perturbative interactions between heavy quarks and quark-gluon plasma within a unified approach*, *Phys. Lett. B* **838** (2023) 137733 [arXiv:2112.15062] [INSPIRE].

[107] D. Zigic et al., *DREENA-A framework as a QGP tomography tool*, *Front. in Phys.* **10** (2022) 957019 [arXiv:2110.01544] [INSPIRE].

[108] S. Stojku et al., *Early evolution constrained by high-p⊥ quark-gluon plasma tomography*, *Phys. Rev. C* **105** (2022) L021901 [arXiv:2008.08987] [INSPIRE].

[109] S. Dulat et al., *New parton distribution functions from a global analysis of quantum chromodynamics*, *Phys. Rev. D* **93** (2016) 033006 [arXiv:1506.07443] [INSPIRE].

[110] K.J. Eskola, P. Paakkinen, H. Paukkunen and C.A. Salgado, *EPPS16: Nuclear parton distributions with LHC data*, *Eur. Phys. J. C* **77** (2017) 163 [arXiv:1612.05741] [INSPIRE].

[111] S. Cao et al., *Charmed hadron chemistry in relativistic heavy-ion collisions*, *Phys. Lett. B* **807** (2020) 135561 [arXiv:1911.00456] [INSPIRE].

[112] R. Sharma, I. Vitev and B.-W. Zhang, *Light-cone wave function approach to open heavy flavor dynamics in QCD matter*, *Phys. Rev. C* **80** (2009) 054902 [arXiv:0904.0032] [INSPIRE].

[113] V.G. Kartvelishvili, A.K. Likhoded and V.A. Petrov, *On the Fragmentation Functions of Heavy Quarks Into Hadrons*, *Phys. Lett. B* **78** (1978) 615 [INSPIRE].

[114] ALICE collaboration, *ALICE upgrades during the LHC Long Shutdown 2*, arXiv:2302.01238 [INSPIRE].

JHEP02(2024)066

The ALICE collaboration

S. Acharya[128], D. Adamová[87], G. Aglieri Rinella[33], M. Agnello[30], N. Agrawal[52], Z. Ahammed[136], S. Ahmad[16], S.U. Ahn[72], I. Ahuja[38], A. Akindinov[142], M. Al-Turany[98], D. Aleksandrov[142], B. Alessandro[57], H.M. Alfanda[6], R. Alfaro Molina[68], B. Ali[16], A. Alici[26], N. Alizadehvandchali[117], A. Alkin[33], J. Alme[21], G. Alocco[53], T. Alt[65], A.R. Altamura[51], I. Altsybeev[96], J.R. Alvarado[45], M.N. Anaam[6], C. Andrei[46], N. Andreou[116], A. Andronic[127], V. Anguelov[95], F. Antinori[55], P. Antonioli[52], N. Apadula[75], L. Aphecetche[104], H. Appelshäuser[65], C. Arata[74], S. Arcelli[26], M. Aresti[23], R. Arnaldi[57], J.G.M.C.A. Arneiro[111], I.C. Arsene[20], M. Arslandok[139], A. Augustinus[33], R. Averbeck[98], M.D. Azmi[16], H. Baba[125], A. Badalà[54], J. Bae[105], Y.W. Baek[41], X. Bai[121], R. Bailhache[65], Y. Bailung[49], A. Balbino[30], A. Baldisseri[131], B. Balis[2], D. Banerjee[4], Z. Banoo[92], R. Barbera[27], F. Barile[32], L. Barioglio[96], M. Barlou[79], B. Barman[42], G.G. Barnaföldi[47], L.S. Barnby[86], V. Barret[128], L. Barreto[111], C. Bartels[120], K. Barth[33], E. Bartsch[65], N. Bastid[128], S. Basu[76], G. Batigne[104], D. Battistini[96], B. Batyunya[143], D. Bauri[48], J.L. Bazo Alba[102], I.G. Bearden[84], C. Beattie[139], P. Becht[98], D. Behera[49], I. Belikov[130], A.D.C. Bell Hechavarria[127], F. Bellini[26], R. Bellwied[117], S. Belokurova[142], Y.A.V. Beltran[45], G. Bencedi[47], S. Beole[25], Y. Berdnikov[142], A. Berdnikova[95], L. Bergmann[95], M.G. Besoiu[64], L. Betev[33], P.P. Bhaduri[136], A. Bhasin[92], M.A. Bhat[4], B. Bhattacharjee[42], L. Bianchi[25], N. Bianchi[50], J. Bielčík[36], J. Bielčíková[87], J. Biernat[108], A.P. Bigot[130], A. Bilandzic[96], G. Biro[47], S. Biswas[4], N. Bize[104], J.T. Blair[109], D. Blau[142], M.B. Blidaru[98], N. Bluhme[39], C. Blume[65], G. Boca[22,56], F. Bock[88], T. Bodova[21], A. Bogdanov[142], S. Boi[23], J. Bok[59], L. Boldizsár[47], M. Bombara[38], P.M. Bond[33], G. Bonomi[135,56], H. Borel[131], A. Borissov[142], A.G. Borquez Carcamo[95], H. Bossi[139], E. Botta[25], Y.E.M. Bouziani[65], L. Bratrud[65], P. Braun-Munzinger[98], M. Bregant[111], M. Broz[36], G.E. Bruno[97,32], M.D. Buckland[24], D. Budnikov[142], H. Buesching[65], S. Bufalino[30], P. Buhler[103], N. Burmasov[142], Z. Buthelezi[69,124], A. Bylinkin[21], S.A. Bysiak[108], M. Cai[6], H. Caines[139], A. Caliva[29], E. Calvo Villar[102], J.M.M. Camacho[110], P. Camerini[24], F.D.M. Canedo[111], S.L. Cantway[139], M. Carabas[114], A.A. Carballo[33], F. Carnesecchi[33], R. Caron[129], L.A.D. Carvalho[111], J. Castillo Castellanos[131], F. Catalano[33,25], C. Ceballos Sanchez[143], I. Chakaberia[75], P. Chakraborty[48], S. Chandra[136], S. Chapeland[33], M. Chartier[120], S. Chattopadhyay[136], S. Chattopadhyay[100], T. Cheng[98,6], C. Cheshkov[129], B. Cheynis[129], V. Chibante Barroso[33], D.D. Chinellato[112], E.S. Chizzali[96,II], J. Cho[59], S. Cho[59], P. Chochula[33], D. Choudhury[42], P. Christakoglou[85], C.H. Christensen[84], P. Christiansen[76], T. Chujo[126], M. Ciacco[30], C. Cicalo[53], F. Cindolo[52], M.R. Ciupek[98], G. Clai[52,III], F. Colamaria[51], J.S. Colburn[101], D. Colella[97,32], M. Colocci[26], M. Concas[33,IV], G. Conesa Balbastre[74], Z. Conesa del Valle[132], G. Contin[24], J.G. Contreras[36], M.L. Coquet[131], P. Cortese[134,57], M.R. Cosentino[113], F. Costa[33], S. Costanza[22,56], C. Cot[132], J. Crkovská[95], P. Crochet[128], R. Cruz-Torres[75], P. Cui[6], A. Dainese[55], M.C. Danisch[95], A. Danu[64], P. Das[81], P. Das[4], S. Das[4], A.R. Dash[127], S. Dash[48], A. De Caro[29], G. de Cataldo[51], J. de Cuveland[39], A. De Falco[23], D. De Gruttola[29], N. De Marco[57], C. De Martin[24], S. De Pasquale[29], R. Deb[135], R. Del Grande[96], L. Dello Stritto[29], W. Deng[6],

JHEP02(2024)066

P. Dhankher[19], D. Di Bari[32], A. Di Mauro[33], B. Diab[131], R.A. Diaz[143,7], T. Dietel[115], Y. Ding[6], J. Ditzel[65], R. Divià[33], D.U. Dixit[19], Ø. Djuvsland[21], U. Dmitrieva[142], A. Dobrin[64], B. Dönigus[65], J.M. Dubinski[137], A. Dubla[98], S. Dudi[91], P. Dupieux[128], M. Durkac[107], N. Dzalaiova[13], T.M. Eder[127], R.J. Ehlers[75], F. Eisenhut[65], R. Ejima[93], D. Elia[51], B. Erazmus[104], F. Ercolessi[26], B. Espagnon[132], G. Eulisse[33], D. Evans[101], S. Evdokimov[142], L. Fabbietti[96], M. Faggin[28], J. Faivre[74], F. Fan[6], W. Fan[75], A. Fantoni[50], M. Fasel[88], A. Feliciello[57], G. Feofilov[142], A. Fernández Téllez[45], L. Ferrandi[111], M.B. Ferrer[33], A. Ferrero[131], C. Ferrero[57], A. Ferretti[25], V.J.G. Feuillard[95], V. Filova[36], D. Finogeev[142], F.M. Fionda[53], E. Flatland[33], F. Flor[117], A.N. Flores[109], S. Foertsch[69], I. Fokin[95], S. Fokin[142], E. Fragiacomo[58], E. Frajna[47], U. Fuchs[33], N. Funicello[29], C. Furget[74], A. Furs[142], T. Fusayasu[99], J.J. Gaardhøje[84], M. Gagliardi[25], A.M. Gago[102], T. Gahlaut[48], C.D. Galvan[110], D.R. Gangadharan[117], P. Ganoti[79], C. Garabatos[98], T. García Chávez[45], E. Garcia-Solis[9], C. Gargiulo[33], P. Gasik[98], A. Gautam[119], M.B. Gay Ducati[67], M. Germain[104], A. Ghimouz[126], C. Ghosh[136], M. Giacalone[52], G. Gioachin[30], P. Giubellino[98,57], P. Giubilato[28], A.M.C. Glaenzer[131], P. Glässel[95], E. Glimos[123], D.J.Q. Goh[77], V. Gonzalez[138], P. Gordeev[142], M. Gorgon[2], K. Goswami[49], S. Gotovac[34], V. Grabski[68], L.K. Graczykowski[137], E. Grecka[87], A. Grelli[60], C. Grigoras[33], V. Grigoriev[142], S. Grigoryan[143,1], F. Grosa[33], J.F. Grosse-Oetringhaus[33], R. Grosso[98], D. Grund[36], N.A. Grunwald[95], G.G. Guardiano[112], R. Guernane[74], M. Guilbaud[104], K. Gulbrandsen[84], T. Gündem[65], T. Gunji[125], W. Guo[6], A. Gupta[92], R. Gupta[92], R. Gupta[49], K. Gwizdziel[137], L. Gyulai[47], C. Hadjidakis[132], F.U. Haider[92], S. Haidlova[36], H. Hamagaki[77], A. Hamdi[75], Y. Han[140], B.G. Hanley[138], R. Hannigan[109], J. Hansen[76], M.R. Haque[137], J.W. Harris[139], A. Harton[9], H. Hassan[118], D. Hatzifotiadou[52], P. Hauer[43], L.B. Havener[139], S.T. Heckel[96], E. Hellbär[98], H. Helstrup[35], M. Hemmer[65], T. Herman[36], G. Herrera Corral[8], F. Herrmann[127], S. Herrmann[129], K.F. Hetland[35], B. Heybeck[65], H. Hillemanns[33], B. Hippolyte[130], F.W. Hoffmann[71], B. Hofman[60], G.H. Hong[140], M. Horst[96], A. Horzyk[2], Y. Hou[6], P. Hristov[33], C. Hughes[123], P. Huhn[65], L.M. Huhta[118], T.J. Humanic[89], A. Hutson[117], D. Hutter[39], R. Ilkaev[142], H. Ilyas[14], M. Inaba[126], G.M. Innocenti[33], M. Ippolitov[142], A. Isakov[85,87], T. Isidori[119], M.S. Islam[100], M. Ivanov[13], M. Ivanov[98], V. Ivanov[142], K.E. Iversen[76], M. Jablonski[2], B. Jacak[75], N. Jacazio[26], P.M. Jacobs[75], S. Jadlovska[107], J. Jadlovsky[107], S. Jaelani[83], C. Jahnke[111], M.J. Jakubowska[137], M.A. Janik[137], T. Janson[71], S. Ji[17], S. Jia[10], A.A.P. Jimenez[66], F. Jonas[88,127], D.M. Jones[120], J.M. Jowett[33,98], J. Jung[65], M. Jung[65], A. Junique[33], A. Jusko[101], M.J. Kabus[33,137], J. Kaewjai[106], P. Kalinak[61], A.S. Kalteyer[98], A. Kalweit[33], V. Kaplin[142], A. Karasu Uysal[73], D. Karatovic[90], O. Karavichev[142], T. Karavicheva[142], P. Karczmarczyk[137], E. Karpechev[142], U. Kebschull[71], R. Keidel[141], D.L.D. Keijdener[60], M. Keil[33], B. Ketzer[43], S.S. Khade[49], A.M. Khan[121], S. Khan[16], A. Khanzadeev[142], Y. Kharlov[142], A. Khatun[119], A. Khuntia[36], B. Kileng[35], B. Kim[105], C. Kim[17], D.J. Kim[118], E.J. Kim[70], J. Kim[140], J.S. Kim[41], J. Kim[59], J. Kim[70], M. Kim[19], S. Kim[18], T. Kim[140], K. Kimura[93], S. Kirsch[65], I. Kisel[39], S. Kiselev[142], A. Kisiel[137], J.P. Kitowski[2], J.L. Klay[5], J. Klein[33], S. Klein[75], C. Klein-Bösing[127], M. Kleiner[65], T. Klemenz[96], A. Kluge[33], A.G. Knospe[117], C. Kobdaj[106], T. Kollegger[98],

JHEP02(2024)066

A. Kondratyev[143], N. Kondratyeva[142], E. Kondratyuk[142], J. Konig[65], S.A. Konigstorfer[96], P.J. Konopka[33], G. Kornakov[137], M. Korwieser[96], S.D. Koryciak[2], A. Kotliarov[87], V. Kovalenko[142], M. Kowalski[108], V. Kozhuharov[37], I. Králik[61], A. Kravčáková[38], L. Krcal[33,39], M. Krivda[101,61], F. Krizek[87], K. Krizkova Gajdosova[33], M. Kroesen[95], M. Krüger[65], D.M. Krupova[36], E. Kryshen[142], V. Kučera[59], C. Kuhn[130], P.G. Kuijer[85], T. Kumaoka[126], D. Kumar[136], L. Kumar[91], N. Kumar[91], S. Kumar[32], S. Kundu[33], P. Kurashvili[80], A. Kurepin[142], A.B. Kurepin[142], A. Kuryakin[142], S. Kushpil[87], V. Kuskov[142], M.J. Kweon[59], Y. Kwon[140], S.L. La Pointe[39], P. La Rocca[27], A. Lakrathok[106], M. Lamanna[33], A.R. Landou[74,116], R. Langoy[122], P. Larionov[33], E. Laudi[33], L. Lautner[33,96], R. Lavicka[103], R. Lea[135,56], H. Lee[105], I. Legrand[46], G. Legras[127], J. Lehrbach[39], T.M. Lelek[2], R.C. Lemmon[86], I. León Monzón[110], M.M. Lesch[96], E.D. Lesser[19], P. Lévai[47], X. Li[10], J. Lien[122], R. Lietava[101], I. Likmeta[117], B. Lim[25], S.H. Lim[17], V. Lindenstruth[39], A. Lindner[46], C. Lippmann[98], D.H. Liu[6], J. Liu[120], G.S.S. Liveraro[112], I.M. Lofnes[21], C. Loizides[88], S. Lokos[108], J. Lömker[60], P. Loncar[34], X. Lopez[128], E. López Torres[7], P. Lu[98,121], F.V. Lugo[68], J.R. Luhder[127], M. Lunardon[28], G. Luparello[58], Y.G. Ma[40], M. Mager[33], A. Maire[130], E.M. Majerz[2], M.V. Makariev[37], M. Malaev[142], G. Malfattore[26], N.M. Malik[92], Q.W. Malik[20], S.K. Malik[92], L. Malinina[143,I,VII], D. Mallick[132,81], N. Mallick[49], G. Mandaglio[31,54], S.K. Mandal[80], V. Manko[142], F. Manso[128], V. Manzari[51], Y. Mao[6], R.W. Marcjan[2], G.V. Margagliotti[24], A. Margotti[52], A. Marín[98], C. Markert[109], P. Martinengo[33], M.I. Martínez[45], G. Martínez García[104], M.P.P. Martins[111], S. Masciocchi[98], M. Masera[25], A. Masoni[53], L. Massacrier[132], O. Massen[60], A. Mastroserio[133,51], O. Matonoha[76], S. Mattiazzo[28], A. Matyja[108], C. Mayer[108], A.L. Mazuecos[33], F. Mazzaschi[25], M. Mazzilli[33], J.E. Mdhluli[124], Y. Melikyan[44], A. Menchaca-Rocha[68], J.E.M. Mendez[66], E. Meninno[103], A.S. Menon[117], M. Meres[13], S. Mhlanga[115,69], Y. Miake[126], L. Micheletti[33], D.L. Mihaylov[96], K. Mikhaylov[143,142], A.N. Mishra[47], D. Miśkowiec[98], A. Modak[4], B. Mohanty[81], M. Mohisin Khan[16,V], M.A. Molander[44], S. Monira[137], C. Mordasini[118], D.A. Moreira De Godoy[127], I. Morozov[142], A. Morsch[33], T. Mrnjavac[33], V. Muccifora[50], S. Muhuri[136], J.D. Mulligan[75], A. Mulliri[23], M.G. Munhoz[111], R.H. Munzer[65], H. Murakami[125], S. Murray[115], L. Musa[33], J. Musinsky[61], J.W. Myrcha[137], B. Naik[124], A.I. Nambrath[19], B.K. Nandi[48], R. Nania[52], E. Nappi[51], A.F. Nassirpour[18], A. Nath[95], C. Nattrass[123], M.N. Naydenov[37], A. Neagu[20], A. Negru[114], E. Nekrasova[142], L. Nellen[66], R. Nepeivoda[76], S. Nese[20], G. Neskovic[39], N. Nicassio[51], B.S. Nielsen[84], E.G. Nielsen[84], S. Nikolaev[142], S. Nikulin[142], V. Nikulin[142], F. Noferini[52], S. Noh[12], P. Nomokonov[143], J. Norman[120], N. Novitzky[88], P. Nowakowski[137], A. Nyanin[142], J. Nystrand[21], M. Ogino[77], S. Oh[18], A. Ohlson[76], V.A. Okorokov[142], J. Oleniacz[137], A.C. Oliveira Da Silva[123], A. Onnerstad[118], C. Oppedisano[57], A. Ortiz Velasquez[66], J. Otwinowski[108], M. Oya[93], K. Oyama[77], Y. Pachmayer[95], S. Padhan[48], D. Pagano[135,56], G. Paić[66], S. Paisano-Guzmán[45], A. Palasciano[51], S. Panebianco[131], H. Park[126], H. Park[105], J. Park[59], J.E. Parkkila[33], Y. Patley[48], R.N. Patra[92], B. Paul[23], H. Pei[6], T. Peitzmann[60], X. Peng[11], M. Pennisi[25], S. Perciballi[25], D. Peresunko[142], G.M. Perez[7], Y. Pestov[142], V. Petrov[142], M. Petrovici[46], R.P. Pezzi[104,67], S. Piano[58], M. Pikna[13], P. Pillot[104], O. Pinazza[52,33], L. Pinsky[117], C. Pinto[96], S. Pisano[50], M. Płoskoń[75],

JHEP02(2024)066

M. Planinic[90], F. Pliquett[65], M.G. Poghosyan[88], B. Polichtchouk[142], S. Politano[30], N. Poljak[90], A. Pop[46], S. Porteboeuf-Houssais[128], V. Pozdniakov[143], I.Y. Pozos[45], K.K. Pradhan[49], S.K. Prasad[4], S. Prasad[49], R. Preghenella[52], F. Prino[57], C.A. Pruneau[138], I. Pshenichnov[142], M. Puccio[33], S. Pucillo[25], Z. Pugelova[107], S. Qiu[85], L. Quaglia[25], S. Ragoni[15], A. Rai[139], A. Rakotozafindrabe[131], L. Ramello[134,57], F. Rami[130], T.A. Rancien[74], M. Rasa[27], S.S. Räsänen[44], R. Rath[52], M.P. Rauch[21], I. Ravasenga[85], K.F. Read[88,123], C. Reckziegel[113], A.R. Redelbach[39], K. Redlich[80,VI], C.A. Reetz[98], H.D. Regules-Medel[45], A. Rehman[21], F. Reidt[33], H.A. Reme-Ness[35], Z. Rescakova[38], K. Reygers[95], A. Riabov[142], V. Riabov[142], R. Ricci[29], M. Richter[20], A.A. Riedel[96], W. Riegler[33], A.G. Riffero[25], C. Ristea[64], M.V. Rodriguez[33], M. Rodríguez Cahuantzi[45], S.A. Rodríguez Ramírez[45], K. Røed[20], R. Rogalev[142], E. Rogochaya[143], T.S. Rogoschinski[65], D. Rohr[33], D. Röhrich[21], P.F. Rojas[45], S. Rojas Torres[36], P.S. Rokita[137], G. Romanenko[26], F. Ronchetti[50], A. Rosano[31,54], E.D. Rosas[66], K. Roslon[137], A. Rossi[55], A. Roy[49], S. Roy[48], N. Rubini[26], D. Ruggiano[137], R. Rui[24], P.G. Russek[2], R. Russo[85], A. Rustamov[82], E. Ryabinkin[142], Y. Ryabov[142], A. Rybicki[108], H. Rytkonen[118], J. Ryu[17], W. Rzesa[137], O.A.M. Saarimaki[44], S. Sadhu[32], S. Sadovsky[142], J. Saetre[21], K. Šafařík[36], P. Saha[42], S.K. Saha[4], S. Saha[81], B. Sahoo[48], B. Sahoo[49], R. Sahoo[49], S. Sahoo[62], D. Sahu[49], P.K. Sahu[62], J. Saini[136], K. Sajdakova[38], S. Sakai[126], M.P. Salvan[98], S. Sambyal[92], D. Samitz[103], I. Sanna[33,96], T.B. Saramela[111], P. Sarma[42], V. Sarritzu[23], V.M. Sarti[96], M.H.P. Sas[33], S. Sawan[81], J. Schambach[88], H.S. Scheid[65], C. Schiaua[46], R. Schicker[95], F. Schlepper[95], A. Schmah[98], C. Schmidt[98], H.R. Schmidt[94], M.O. Schmidt[33], M. Schmidt[94], N.V. Schmidt[88], A.R. Schmier[123], R. Schotter[130], A. Schröter[39], J. Schukraft[33], K. Schweda[98], G. Scioli[26], E. Scomparin[57], J.E. Seger[15], Y. Sekiguchi[125], D. Sekihata[125], M. Selina[85], I. Selyuzhenkov[98], S. Senyukov[130], J.J. Seo[95,59], D. Serebryakov[142], L. Šerkšnytė[96], A. Sevcenco[64], T.J. Shaba[69], A. Shabetai[104], R. Shahoyan[33], A. Shangaraev[142], A. Sharma[91], B. Sharma[92], D. Sharma[48], H. Sharma[55], M. Sharma[92], S. Sharma[77], S. Sharma[92], U. Sharma[92], A. Shatat[132], O. Sheibani[117], K. Shigaki[93], M. Shimomura[78], J. Shin[12], S. Shirinkin[142], Q. Shou[40], Y. Sibiriak[142], S. Siddhanta[53], T. Siemiarczuk[80], T.F. Silva[111], D. Silvermyr[76], T. Simantathammakul[106], R. Simeonov[37], B. Singh[92], B. Singh[96], K. Singh[49], R. Singh[81], R. Singh[92], R. Singh[49], S. Singh[16], V.K. Singh[136], V. Singhal[136], T. Sinha[100], B. Sitar[13], M. Sitta[134,57], T.B. Skaali[20], G. Skorodumovs[95], M. Slupecki[44], N. Smirnov[139], R.J.M. Snellings[60], E.H. Solheim[20], J. Song[17], C. Sonnabend[33,98], F. Soramel[28], A.B. Soto-hernandez[89], R. Spijkers[85], I. Sputowska[108], J. Staa[76], J. Stachel[95], I. Stan[64], P.J. Steffanic[123], S.F. Stiefelmaier[95], D. Stocco[104], I. Storehaug[20], P. Stratmann[127], S. Strazzi[26], A. Sturniolo[31,54], C.P. Stylianidis[85], A.A.P. Suaide[111], C. Suire[132], M. Sukhanov[142], M. Suljic[33], R. Sultanov[142], V. Sumberia[92], S. Sumowidagdo[83], S. Swain[62], I. Szarka[13], M. Szymkowski[137], S.F. Taghavi[96], G. Taillepied[98], J. Takahashi[112], G.J. Tambave[81], S. Tang[6], Z. Tang[121], J.D. Tapia Takaki[119], N. Tapus[114], L.A. Tarasovicova[127], M.G. Tarzila[46], G.F. Tassielli[32], A. Tauro[33], A. Tavira García[132], G. Tejeda Muñoz[45], A. Telesca[33], L. Terlizzi[25], C. Terrevoli[117], S. Thakur[4], D. Thomas[109], A. Tikhonov[142], N. Tiltmann[127], A.R. Timmins[117], M. Tkacik[107], T. Tkacik[107], A. Toia[65], R. Tokumoto[93], K. Tomohiro[93], N. Topilskaya[142],

JHEP02(2024)066

M. Toppi[50], T. Tork[132], V.V. Torres[104], A.G. Torres Ramos[32], A. Trifiró[31,54], A.S. Triolo[33,31,54], S. Tripathy[52], T. Tripathy[48], S. Trogolo[33], V. Trubnikov[3], W.H. Trzaska[118], T.P. Trzcinski[137], A. Tumkin[142], R. Turrisi[55], T.S. Tveter[20], K. Ullaland[21], B. Ulukutlu[96], A. Uras[129], G.L. Usai[23], M. Vala[38], N. Valle[22], L.V.R. van Doremalen[60], M. van Leeuwen[85], C.A. van Veen[95], R.J.G. van Weelden[85], P. Vande Vyvre[33], D. Varga[47], Z. Varga[47], P. Vargas Torres[66], M. Vasileiou[79], A. Vasiliev[142], O. Vázquez Doce[50], O. Vazquez Rueda[117], V. Vechernin[142], E. Vercellin[25], S. Vergara Limón[45], R. Verma[48], L. Vermunt[98], R. Vértesi[47], M. Verweij[60], L. Vickovic[34], Z. Vilakazi[124], O. Villalobos Baillie[101], A. Villani[24], A. Vinogradov[142], T. Virgili[29], M.M.O. Virta[118], V. Vislavicius[76], A. Vodopyanov[143], B. Volkel[33], M.A. Völkl[95], K. Voloshin[142], S.A. Voloshin[138], G. Volpe[32], B. von Haller[33], I. Vorobyev[96], N. Vozniuk[142], J. Vrláková[38], J. Wan[40], C. Wang[40], D. Wang[40], Y. Wang[40], Y. Wang[6], A. Wegrzynek[33], F.T. Weiglhofer[39], S.C. Wenzel[33], J.P. Wessels[127], J. Wiechula[65], J. Wikne[20], G. Wilk[80], J. Wilkinson[98], G.A. Willems[127], B. Windelband[95], M. Winn[131], J.R. Wright[109], W. Wu[40], Y. Wu[121], R. Xu[6], A. Yadav[43], A.K. Yadav[136], S. Yalcin[73], Y. Yamaguchi[93], S. Yang[21], S. Yano[93], Z. Yin[6], I.-K. Yoo[17], J.H. Yoon[59], H. Yu[12], S. Yuan[21], A. Yuncu[95], V. Zaccolo[24], C. Zampolli[33], F. Zanone[95], N. Zardoshti[33], A. Zarochentsev[142], P. Závada[63], N. Zaviyalov[142], M. Zhalov[142], B. Zhang[6], C. Zhang[131], L. Zhang[40], S. Zhang[40], X. Zhang[6], Y. Zhang[121], Z. Zhang[6], M. Zhao[10], V. Zherebchevskii[142], Y. Zhi[10], D. Zhou[6], Y. Zhou[84], J. Zhu[55,6], Y. Zhu[6], S.C. Zugravel[57], N. Zurlo[135,56]

[1] *A.I. Alikhanyan National Science Laboratory (Yerevan Physics Institute) Foundation, Yerevan, Armenia*
[2] *AGH University of Krakow, Cracow, Poland*
[3] *Bogolyubov Institute for Theoretical Physics, National Academy of Sciences of Ukraine, Kiev, Ukraine*
[4] *Bose Institute, Department of Physics and Centre for Astroparticle Physics and Space Science (CAPSS), Kolkata, India*
[5] *California Polytechnic State University, San Luis Obispo, California, U.S.A.*
[6] *Central China Normal University, Wuhan, China*
[7] *Centro de Aplicaciones Tecnológicas y Desarrollo Nuclear (CEADEN), Havana, Cuba*
[8] *Centro de Investigación y de Estudios Avanzados (CINVESTAV), Mexico City and Mérida, Mexico*
[9] *Chicago State University, Chicago, Illinois, U.S.A.*
[10] *China Institute of Atomic Energy, Beijing, China*
[11] *China University of Geosciences, Wuhan, China*
[12] *Chungbuk National University, Cheongju, Republic of Korea*
[13] *Comenius University Bratislava, Faculty of Mathematics, Physics and Informatics, Bratislava, Slovak Republic*
[14] *COMSATS University Islamabad, Islamabad, Pakistan*
[15] *Creighton University, Omaha, Nebraska, U.S.A.*
[16] *Department of Physics, Aligarh Muslim University, Aligarh, India*
[17] *Department of Physics, Pusan National University, Pusan, Republic of Korea*
[18] *Department of Physics, Sejong University, Seoul, Republic of Korea*
[19] *Department of Physics, University of California, Berkeley, California, U.S.A.*
[20] *Department of Physics, University of Oslo, Oslo, Norway*
[21] *Department of Physics and Technology, University of Bergen, Bergen, Norway*
[22] *Dipartimento di Fisica, Università di Pavia, Pavia, Italy*
[23] *Dipartimento di Fisica dell'Università and Sezione INFN, Cagliari, Italy*
[24] *Dipartimento di Fisica dell'Università and Sezione INFN, Trieste, Italy*
[25] *Dipartimento di Fisica dell'Università and Sezione INFN, Turin, Italy*
[26] *Dipartimento di Fisica e Astronomia dell'Università and Sezione INFN, Bologna, Italy*

JHEP02(2024)066

[27] Dipartimento di Fisica e Astronomia dell'Università and Sezione INFN, Catania, Italy
[28] Dipartimento di Fisica e Astronomia dell'Università and Sezione INFN, Padova, Italy
[29] Dipartimento di Fisica 'E.R. Caianiello' dell'Università and Gruppo Collegato INFN, Salerno, Italy
[30] Dipartimento DISAT del Politecnico and Sezione INFN, Turin, Italy
[31] Dipartimento di Scienze MIFT, Università di Messina, Messina, Italy
[32] Dipartimento Interateneo di Fisica 'M. Merlin' and Sezione INFN, Bari, Italy
[33] European Organization for Nuclear Research (CERN), Geneva, Switzerland
[34] Faculty of Electrical Engineering, Mechanical Engineering and Naval Architecture, University of Split, Split, Croatia
[35] Faculty of Engineering and Science, Western Norway University of Applied Sciences, Bergen, Norway
[36] Faculty of Nuclear Sciences and Physical Engineering, Czech Technical University in Prague, Prague, Czech Republic
[37] Faculty of Physics, Sofia University, Sofia, Bulgaria
[38] Faculty of Science, P.J. Šafárik University, Košice, Slovak Republic
[39] Frankfurt Institute for Advanced Studies, Johann Wolfgang Goethe-Universität Frankfurt, Frankfurt, Germany
[40] Fudan University, Shanghai, China
[41] Gangneung-Wonju National University, Gangneung, Republic of Korea
[42] Gauhati University, Department of Physics, Guwahati, India
[43] Helmholtz-Institut für Strahlen- und Kernphysik, Rheinische Friedrich-Wilhelms-Universität Bonn, Bonn, Germany
[44] Helsinki Institute of Physics (HIP), Helsinki, Finland
[45] High Energy Physics Group, Universidad Autónoma de Puebla, Puebla, Mexico
[46] Horia Hulubei National Institute of Physics and Nuclear Engineering, Bucharest, Romania
[47] HUN-REN Wigner Research Centre for Physics, Budapest, Hungary
[48] Indian Institute of Technology Bombay (IIT), Mumbai, India
[49] Indian Institute of Technology Indore, Indore, India
[50] INFN, Laboratori Nazionali di Frascati, Frascati, Italy
[51] INFN, Sezione di Bari, Bari, Italy
[52] INFN, Sezione di Bologna, Bologna, Italy
[53] INFN, Sezione di Cagliari, Cagliari, Italy
[54] INFN, Sezione di Catania, Catania, Italy
[55] INFN, Sezione di Padova, Padova, Italy
[56] INFN, Sezione di Pavia, Pavia, Italy
[57] INFN, Sezione di Torino, Turin, Italy
[58] INFN, Sezione di Trieste, Trieste, Italy
[59] Inha University, Incheon, Republic of Korea
[60] Institute for Gravitational and Subatomic Physics (GRASP), Utrecht University/Nikhef, Utrecht, The Netherlands
[61] Institute of Experimental Physics, Slovak Academy of Sciences, Košice, Slovak Republic
[62] Institute of Physics, Homi Bhabha National Institute, Bhubaneswar, India
[63] Institute of Physics of the Czech Academy of Sciences, Prague, Czech Republic
[64] Institute of Space Science (ISS), Bucharest, Romania
[65] Institut für Kernphysik, Johann Wolfgang Goethe-Universität Frankfurt, Frankfurt, Germany
[66] Instituto de Ciencias Nucleares, Universidad Nacional Autónoma de México, Mexico City, Mexico
[67] Instituto de Física, Universidade Federal do Rio Grande do Sul (UFRGS), Porto Alegre, Brazil
[68] Instituto de Física, Universidad Nacional Autónoma de México, Mexico City, Mexico
[69] iThemba LABS, National Research Foundation, Somerset West, South Africa
[70] Jeonbuk National University, Jeonju, Republic of Korea
[71] Johann-Wolfgang-Goethe Universität Frankfurt Institut für Informatik, Fachbereich Informatik und Mathematik, Frankfurt, Germany
[72] Korea Institute of Science and Technology Information, Daejeon, Republic of Korea
[73] KTO Karatay University, Konya, Turkey

JHEP02(2024)066

[74] *Laboratoire de Physique Subatomique et de Cosmologie, Université Grenoble-Alpes, CNRS-IN2P3, Grenoble, France*
[75] *Lawrence Berkeley National Laboratory, Berkeley, California, U.S.A.*
[76] *Lund University Department of Physics, Division of Particle Physics, Lund, Sweden*
[77] *Nagasaki Institute of Applied Science, Nagasaki, Japan*
[78] *Nara Women's University (NWU), Nara, Japan*
[79] *National and Kapodistrian University of Athens, School of Science, Department of Physics, Athens, Greece*
[80] *National Centre for Nuclear Research, Warsaw, Poland*
[81] *National Institute of Science Education and Research, Homi Bhabha National Institute, Jatni, India*
[82] *National Nuclear Research Center, Baku, Azerbaijan*
[83] *National Research and Innovation Agency - BRIN, Jakarta, Indonesia*
[84] *Niels Bohr Institute, University of Copenhagen, Copenhagen, Denmark*
[85] *Nikhef, National institute for subatomic physics, Amsterdam, Netherlands*
[86] *Nuclear Physics Group, STFC Daresbury Laboratory, Daresbury, U.K.*
[87] *Nuclear Physics Institute of the Czech Academy of Sciences, Husinec-Řež, Czech Republic*
[88] *Oak Ridge National Laboratory, Oak Ridge, Tennessee, U.S.A.*
[89] *Ohio State University, Columbus, Ohio, U.S.A.*
[90] *Physics department, Faculty of science, University of Zagreb, Zagreb, Croatia*
[91] *Physics Department, Panjab University, Chandigarh, India*
[92] *Physics Department, University of Jammu, Jammu, India*
[93] *Physics Program and International Institute for Sustainability with Knotted Chiral Meta Matter (SKCM2), Hiroshima University, Hiroshima, Japan*
[94] *Physikalisches Institut, Eberhard-Karls-Universität Tübingen, Tübingen, Germany*
[95] *Physikalisches Institut, Ruprecht-Karls-Universität Heidelberg, Heidelberg, Germany*
[96] *Physik Department, Technische Universität München, Munich, Germany*
[97] *Politecnico di Bari and Sezione INFN, Bari, Italy*
[98] *Research Division and ExtreMe Matter Institute EMMI, GSI Helmholtzzentrum für Schwerionenforschung GmbH, Darmstadt, Germany*
[99] *Saga University, Saga, Japan*
[100] *Saha Institute of Nuclear Physics, Homi Bhabha National Institute, Kolkata, India*
[101] *School of Physics and Astronomy, University of Birmingham, Birmingham, U.K.*
[102] *Sección Física, Departamento de Ciencias, Pontificia Universidad Católica del Perú, Lima, Peru*
[103] *Stefan Meyer Institut für Subatomare Physik (SMI), Vienna, Austria*
[104] *SUBATECH, IMT Atlantique, Nantes Université, CNRS-IN2P3, Nantes, France*
[105] *Sungkyunkwan University, Suwon City, Republic of Korea*
[106] *Suranaree University of Technology, Nakhon Ratchasima, Thailand*
[107] *Technical University of Košice, Košice, Slovak Republic*
[108] *The Henryk Niewodniczanski Institute of Nuclear Physics, Polish Academy of Sciences, Cracow, Poland*
[109] *The University of Texas at Austin, Austin, Texas, U.S.A.*
[110] *Universidad Autónoma de Sinaloa, Culiacán, Mexico*
[111] *Universidade de São Paulo (USP), São Paulo, Brazil*
[112] *Universidade Estadual de Campinas (UNICAMP), Campinas, Brazil*
[113] *Universidade Federal do ABC, Santo Andre, Brazil*
[114] *Universitatea Nationala de Stiinta si Tehnologie Politehnica Bucuresti, Bucharest, Romania*
[115] *University of Cape Town, Cape Town, South Africa*
[116] *University of Derby, Derby, U.K.*
[117] *University of Houston, Houston, Texas, U.S.A.*
[118] *University of Jyväskylä, Jyväskylä, Finland*
[119] *University of Kansas, Lawrence, Kansas, U.S.A.*
[120] *University of Liverpool, Liverpool, U.K.*
[121] *University of Science and Technology of China, Hefei, China*
[122] *University of South-Eastern Norway, Kongsberg, Norway*
[123] *University of Tennessee, Knoxville, Tennessee, U.S.A.*

JHEP02(2024)066

[124] University of the Witwatersrand, Johannesburg, South Africa
[125] University of Tokyo, Tokyo, Japan
[126] University of Tsukuba, Tsukuba, Japan
[127] Universität Münster, Institut für Kernphysik, Münster, Germany
[128] Université Clermont Auvergne, CNRS/IN2P3, LPC, Clermont-Ferrand, France
[129] Université de Lyon, CNRS/IN2P3, Institut de Physique des 2 Infinis de Lyon, Lyon, France
[130] Université de Strasbourg, CNRS, IPHC UMR 7178, F-67000 Strasbourg, France, Strasbourg, France
[131] Université Paris-Saclay, Centre d'Etudes de Saclay (CEA), IRFU, Département de Physique Nucléaire (DPhN), Saclay, France
[132] Université Paris-Saclay, CNRS/IN2P3, IJCLab, Orsay, France
[133] Università degli Studi di Foggia, Foggia, Italy
[134] Università del Piemonte Orientale, Vercelli, Italy
[135] Università di Brescia, Brescia, Italy
[136] Variable Energy Cyclotron Centre, Homi Bhabha National Institute, Kolkata, India
[137] Warsaw University of Technology, Warsaw, Poland
[138] Wayne State University, Detroit, Michigan, U.S.A.
[139] Yale University, New Haven, Connecticut, U.S.A.
[140] Yonsei University, Seoul, Republic of Korea
[141] Zentrum für Technologie und Transfer (ZTT), Worms, Germany
[142] Affiliated with an institute covered by a cooperation agreement with CERN
[143] Affiliated with an international laboratory covered by a cooperation agreement with CERN

[I] Deceased
[II] Also at: Max-Planck-Institut fur Physik, Munich, Germany
[III] Also at: Italian National Agency for New Technologies, Energy and Sustainable Economic Development (ENEA), Bologna, Italy
[IV] Also at: Dipartimento DET del Politecnico di Torino, Turin, Italy
[V] Also at: Department of Applied Physics, Aligarh Muslim University, Aligarh, India
[VI] Also at: Institute of Theoretical Physics, University of Wroclaw, Poland
[VII] Also at: An institution covered by a cooperation agreement with CERN

JHEP02(2024)066